TAMPEREEN TEKNILLINEN YLIOPISTO
TAMPERE UNIVERSITY OF TECHNOLOGY
Julkaisu 672 • Publication 672

Rain Ferenets

EEG Patterns and Regularity Properties during Propofol Induced Anesthesia/Sedation

Pori 2007

Tampereen teknillinen yliopisto. Julkaisu 672
Tampere University of Technology. Publication 672

Rain Ferenets

EEG Patterns and Regularity Properties during Propofol Induced Anesthesia/Sedation

Thesis for the degree of Doctor of Technology to be presented with due permission for public examination and criticism in Auditorium 240, at Tampere University of Technology - Pori, on the 31st of August 2007, at 12 noon.

Tampereen teknillinen yliopisto - Tampere University of Technology
Pori 2007

ISBN 978-952-15-1799-0 (printed)
ISBN 978-952-15-1841-6 (PDF)
ISSN 1459-2045

We know accurately only when we know little, with knowledge doubt increases

J. W. von Goethe

Abstract

The purpose of this thesis is to study properties of the EEG signal recorded during anesthesia or sedation. The main emphasis was put on the regularity/complexity analysis of the EEG during gradually deepening sedation and the EEG patterns of burst-suppression level anesthesia. Additionally, time-frequency analysis was applied to selected EEG patterns during burst-suppression level anesthesia. The EEG signals underlying this work have mainly been recorded during propofol anesthesia/sedation, however, for the comparison purposes also sevoflurane recordings have been used. For most of the cases the EEG was recorded using the conventional skin electrodes, however for one case EEG recorded with depth electrodes from the subthalamic region of the brain was used.

Regularity/complexity properties of the signals have been analyzed using several entropy based measures (Shannon entropy, spectral entropy, and approximate entropy), a coarse-grained complexity measure (Lempel-Ziv complexity), and a fractal dimension estimator (Higuchi fractal dimension). The main idea of the regularity/complexity analysis was to study the ability of the different measures to follow the anesthetic depth. In addition, the influence of the frequency content of the EEG signal, as well as co-administration of the commonly used opiate remifentanil, on the efficiency of the mentioned measures as depth-of-sedation indicators was studied. The time-frequency analysis was conducted by using quadratic time-frequency distributions (Wigner-Ville distribution, Choi-Williams distribution, and optimal distributions) in order to investigate the instantaneous frequency of the spindles during propofol induced anesthesia as well as during normal physiological sleep.

The results show that, although the applied regularity/complexity measures do not depend directly on the power spectrum of the signal (with the exception of spectral entropy), they are highly sensitive to the frequency content of the EEG. Higuchi fractal dimension almost always outperformed other measures when their ability to differentiate between different levels of sedation was tested. Remifentanil was found to significantly deteriorate the ability of the tested measures to follow the depth of sedation.

The time-frequency analysis of the spindle patterns shows that the angle of the trend of its instantaneous frequency is generally small. However, occasionally spindles can show either increasing or decreasing trend in the instantaneous frequency. The analysis also reveals that the spindles during propofol anesthesia have slightly higher average frequency than that of the spindles during physiological sleep.

Preface

This work was carried out during the years 2002–2007. I started my studies in Tallinn University of Technology and in 2003 the work was continued in Tampere University of Technology, first in the Ragnar Granit Institute and, thereafter, in the Pori unit.

First and foremost I wish to express my gratitude to professor Tarmo Lipping, for patiently guiding and supporting me through all these years. It was often his enthusiasm and ability to explain things clearly and concisely that gave me some extra encouragement and inspiration to continue during several critical moments.

Special thanks also go to M.D., Ph.D. Ville Jäntti for interestingly explaining several aspects about the EEG and brain functioning. Additionally, I am indebted to him for introducing the basic principles of anesthesiology.

Suggestions and remarks by the official reviewers of the thesis—docent Mark van Gils and professor Lotfi Senahdji—are greatly acknowledged, these helped to improve the overall readability and structure of the thesis.

Many thanks go to M.Sc. Katrina Wendel for finding and correcting grammatical errors in the manuscript of this thesis as well as for giving several useful technical suggestions. All typos found in the text are created afterwards by the author.

Special thanks also go to M.D. Pasi Puumala for many scientific discussions we used to have and for giving me his helping hand during my beginning years in Finland.

I also would like to thank professor emeritus Hiie Hinrikus and Ph.D. Jaanus Lass from the Department of Biomedical Engineering, Tallinn University of Technology. Thanks to them I got involved with such an interesting research field as biomedical signal processing.

I am also indebted to Mr. Väino Kundla and Mr. Enn Nurk—my former teachers of physics and mathematics, respectively—for continuously emphasizing the importance of critical and analytical thinking and, therefore, making my later life considerably easier.

Finally, I would like to thank my wife Marju and son Rainer for continuous support during all these years.

Financial support from the Archimedes Foundation, High Technology Foundation of Satakunta, Finnish Cultural Foundation, and Centre for International Mobility is gratefully acknowledged.

— Rain Ferenets
Tampere, 2007

Contents

List of Original Publications

This thesis is based on the following original publications, hereafter referred to by their Roman numerals:

I R. Ferenets, V. Jäntti, A.-M. Huotari, S. Alahuhta, and T. Lipping. "Comparing Time-Frequency Methods for Estimating Instantaneous Frequency of Spindles during Propofol Anesthesia." In *IFMBE Proceedings*, volume 6, 4 pages, Ischia, Naples, Italy, July 31 – Aug. 5, 2004.

II R. Ferenets, T. Lipping, P. Puumala, V. Jäntti, E. Sonkajärvi, E. Heikkinen, E. Karvonen, and K. Suominen. "Comparing Entropy/Complexity of EEG during Propofol and Sevoflurane Anesthesia at Burst-Suppression Level." In *Proceedings of the 5th International Workshop on Biosignal Interpretation*, pages 187–190, Tokyo, Japan, Sept. 6–8, 2005.

III R. Ferenets, T. Lipping, A. Anier, V. Jäntti, S. Melto, and S. Hovilehti. "Comparison of Entropy and Complexity Measures for the Assessment of Depth of Sedation." *IEEE Transactions on Biomedical Engineering*, **53**(6):1067–1077, 2006.

IV R. Ferenets, T. Lipping, P. Suominen, J. Turunen, P. Puumala, V. Jäntti, S.-L. Himanen, and A.-M. Huotari. "Comparison of the Properties of EEG Spindles in Sleep and Propofol Anesthesia." In *Proceedings of the 28th IEEE EMBS Annual International Conference*, pages 6356–6359, New-York City, USA, Aug. 30 – Sept. 3, 2006.

V R. Ferenets, A. Vanluchene, T. Lipping, B. Heyse, and M. Struys. "Behavior of Entropy/Complexity Measure of the Electroencephalogram during Propofol Induced Sedation: Dose Dependent Effects of Remifentanil." *Anesthesiology*, **106**(4):696–706, 2007.

Supplementary publications related to this work but not included in this thesis:

VI T. Lipping, R. Ferenets, P. Puumala, K. Suominen, E. Karvonen, E. Sonkajärvi, S. Alahuhta, E. Heikkinen, T. Erola, G. Baer, and V. Jäntti. "EEG Independent Component and Coherence Analysis from Scalp and Depth Electrodes During Propofol Anesthesia." In *Proceeedings of the 25th IEEE EMBS Annual International Conference*, pages 2471–2474, Cancun, Mexico, Sept. 17–21, 2003.

VII T. Lipping, R. Ferenets, A. Anier, S. Melto, and S. Hovilehto. "Power Spectrum Estimation in the Calculation of Spectral Entropy to Assess Depth of Sedation." In *The 3rd European Medical & Biological Engineering Conference*, Prague, Czech Republic, Nov. 20–25, 2005.

List of Abbreviations and Symbols

Abbreviations

AF	Ambiguity function
ApEn	Approximate entropy
BIS	Bispectral Index
BJD	Born-Jordan distribution
BS	Burst-suppression
CCD	Cohen's class of distributions
CWD	Choi-Williams distribution
EEG	Electroencephalogram, electroencephalography
FT	Fourier transform
GABA	Gamma-aminobutyric acid
GMCWD	Generalized marginals Choi-Williams distribution
HFD	Higuchi fractal dimension
ICU	Intensive care unit
LZC	Lempel-Ziv complexity
OAA/S	Observer's assessment of alertness/sedation
PDF	Probability density function
PSI	Patient State Index
ShEn	Shannon entropy
SpEn	Spectral entropy
TFD	Time-frequency distribution
WVD	Wigner-Ville distribution

Symbols

α	Alpha rhythm of the EEG signal
β	Beta rhythm of the EEG signal
δ	Delta rhythm of the EEG signal
γ	Gamma rhythm of the EEG signal
$\varkappa$	Number of different symbols in the sequence $\mathbf{s}$
ϕ	Smoothing kernel
Φ^m	Average logarithmic probability of two points being closer than distance r in phase space of dimension m

ψ	Angle of the given branch of GMCWD; angle of the radially Gaussian kernel
σ	Kernel width adjusting parameter
σ_s	Spread function of the radially Gaussian kernel
σ_f	Signal energy spread (resolution) in frequency
σ_t	Signal energy spread (resolution) in time
τ	Time lag
θ	Theta rhythm of the EEG signal
$\Theta(x)$	Heaviside function
ξ	Frequency lag
ζ	Point in the true phase-space
B	Number of branches of GMCWD
b	Normalization factor in LZC algorithm
c	Counter for new pattern in LZC algorithm
C_i^m	Probability of two points being closer than distance r in phase space of dimension m
$C(r)$	Correlation sum
CS_{buf}	Buffer for current sequence in LZC algorithm
D	Fractal dimension; correlation dimension
d	Distance between two phase-space points; distance between AF and the smoothing kernel ϕ
$\mathbf{F}$	Smooth vector field in $\mathbb{R}^d$
f	Frequency
f_{high}	The highest frequency of the given spectrum
f_{low}	The lowest frequency of the given spectrum
h	Measurement function
H_{Sh}	Shannon entropy, not normalized
H_{Sp}	Spectral entropy, not normalized
j	Initial time in the given signal
$\jmath$	Imaginary unit
k	Time interval between samples of a given signal
$k_{\max}$	Maximum value for the time interval k
$L_j(k)$	Length of the subsignal s_j^k
$L(k)$	Average length of all lengths $L_j(k)$
m	Embedding dimension
$\mathcal{N}$	Normalization operation for TFD or smoothing kernel
N	Signal length in samples
N_a	Number of amplitude values in a discrete signal; number of bins in histogram of a discrete signal
N_f	Number of frequency components in given spectrum

P	Power spectrum
p	Probability
PS_{buf}	Buffer for previous sequence in LZC algorithm
r	Maximum allowable distance between two phase-space points
$\mathbb{R}^d$	d-dimensional Euclidean space
$\mathbf{s}$	Sequence of symbols
$s(t)$	Signal in time domain
$s_a(t)$	Analytic signal
$\hat{s}_a(f)$	Fourier transform of the analytic signal s_a
$\hat{s}(f)$	Fourier transform of the non-analytic signal s
s_j^k	Subsignal constructed from the given signal s
T_d	Threshold value for signal conversion in the LZC algorithm
$\mathbf{x}$	Point in the reconstructed phase-space

CHAPTER 1

Introduction

Anesthesia monitoring based on indices calculated from the electroencephalogram (EEG) has been an active area of research field for several decades. The first noticeable success was achieved in 1996 when Aspect Medical Systems, Inc. (USA) introduced the Bispectral Index (BIS). BIS is a method combining several signal processing approaches (frequency, bispectrum, and time domain) for the calculation of a scalar depth of anesthesia measure (Rampil, 1998). From that time on several other commercial methods for the assessment of depth of anesthesia have been developed and implemented. The Patient State Index (PSI) by Physiometrix Inc. (USA), the Narcotrend index by MonitorTechnik (Germany), and the Entropy index by GE Healthcare OY (Finland) can be mentioned as examples (Rampil, 1998; Schultz *et al.*, 2000; Viertiö-Oja *et al.*, 2004; Lipping and Jäntti, 2004; Lipping *et al.*, 2006).

Despite the fact that several different methods/devices are already available for anesthesia monitoring, the research in this field is still very active. There are two main reasons for this: first, the available methods have certain drawbacks causing them to fail in certain situations and, secondly, EEG monitoring is becoming more popular in the intensive care unit (ICU) and the methods designed for monitoring surgical anesthesia may not best suit the situation in the ICU.

On one hand, these depth-of-anesthesia monitors are developed to measure the effect of the anesthetic drug on brain functioning in order to decrease the incidence of awareness in anesthesia, i.e. the situation of too light anesthesia should be avoided (see section 2.2 for the definition of anesthesia). On the other hand, they should help anesthesiologists maintain anesthesia at the optimal level in order to prevent delays in the recovery phase, i.e. too deep anesthesia should be avoided (Senhadji *et al.*, 2002; Recart *et al.*, 2003; Ekman *et al.*, 2004).

The effects of different anesthetics on the EEG are very different. Drugs like propofol and etomidate, which are so-called GABAergic drugs (gamma-aminobutyric acid (GABA) is the principle inhibitory neurotransmitter in the cortex), first cause slowing of the EEG activity and finally a burst-suppression pattern. Other drugs such as ketamine, nitrous oxide and xenon induce unconsciousness with different mechanisms and the EEG changes they produce do not correlate with unconsciousness in the same way as the GABAergic drugs (Nelson *et al.*, 2002; Rudolph and Antkowiak, 2004; Jameson and Sloan, 2006). Thus, for the latter case the earlier mentioned indices calculated from the EEG do not correlate with unconsciousness. Mixtures of the anesthetics such as isoflurane and nitrous oxide, for example, therefore may produce unpredictable behavior in the EEG indices. It has been reported that when the anesthetic drug called ketamine has been used in conjunction with other drugs like propofol or sevoflurane, the

unexpected increase in both BIS and Entropy indices can occur (Hirota *et al.*, 1999; Vereecke *et al.*, 2003; Hans *et al.*, 2005). It has been shown that both BIS and Entropy indices are practically unaffected by the increase of the anesthetic agent nitrous oxide (Barr *et al.*, 1999; Anderson and Jakobsson, 2004; Sleigh and Barnard, 2004). Additionally, Davidson and Czarnecki (2004) have studied the behavior of the BIS in the case of halotane anesthesia in children. The authors concluded that the BIS value should be interpreted with caution since it may underestimate the level of anesthesia.

The manufacturers of the commercial monitors generally provide the range of the corresponding index where the level of anesthesia is considered to be adequate for surgical procedures. Nevertheless, these numbers should be taken critically because there are some cases where awareness during operation (Rampersad and Mulroy, 2005) and explicit recall of the intraoperative events (Mychaskiw *et al.*, 2001) have been reported. However, the depth of anesthesia was adequate according to the BIS monitor for both cases.

EEG monitoring in the ICU helps to optimize the sedation, and therefore, the time period of mechanical ventilation as well as the overall stay in the ICU and hospital can be reduced (Kress *et al.*, 2000; Tonner *et al.*, 2006). Undersedation in the ICU can have several consequences for the patients such as an increased overall stress level, increased blood pressure, and increased oxygen consumption (Roth-Isigkeit *et al.*, 1998; Soliman *et al.*, 2001). Oversedation on the other hand can involve several risks as well. For example, it can cause a decrease in blood pressure, prolonged periods of mechanical ventilation, and withdrawal syndrome for sedative drugs (Cammarano *et al.*, 1998; Tonner *et al.*, 2006).

Anesthesia monitors were initially designed for use in operating rooms, but their use has been extended to the ICU in order to assess the level of sedation (Shapiro, 1999). However, there are some principal differences between the condition of the patients in the ICU and those under surgical anesthesia. While the patients in surgical anesthesia must be unaware of the ongoing events, the ICU patients are tried to be kept at a cooperative level (Tonner *et al.*, 2003). As a consequence, the patients in the ICU usually a have higher level of electromyographic activity which, in turn, can falsely cause increase in the BIS value (Bruhn *et al.*, 2000a). Additionally, in the ICU the recording protocol is normally not as strict as in the operating room, causing usually many more different artifacts. Several studies have evaluated the performance of the BIS index in critically ill patients and found that it is not satisfactory (Nasraway *et al.*, 2002; Riess *et al.*, 2002).

The aim of this thesis is to give an overview of the regularity/complexity as well as the time-frequency methods used in the field of analysis of electrical activity of the brain during anesthesia and sedation and present the original results of the studies performed by the author.

The thesis is organized as follows: Chapter 2 gives an overview of the EEG signal during anesthesia and intensive care. Chapters 3 and 4 review the regularity and complexity measures and the time-frequency methods, respectively, used in this thesis. Chapter 5 presents a brief discussion about the topic and gives a few concluding remarks, as well. Chapter 6 gives a short summary of the original publications as well as the author's contribution. Appendix A gives a brief overview about the history of the term "entropy". A short description of the phase-space concept of the dynamical systems and the correlation dimension is given in appendix B.

CHAPTER 2

EEG Signal during Anesthesia and Intensive Care

This chapter gives a short overview of the EEG signal: its origins, measurement, and classification. Anesthesia and the behavior of the EEG signal during anesthesia is reviewed as well.

2.1 Overview of the EEG Signal

Electroencephalography is the measurement of the electrical activity of the brain by using special electrodes placed on the scalp. The recorded signal is called an electroencephalogram (EEG), and it represents the electrical activity of a large number of neurons in the vicinity of the electrode. In 1924, Hans Berger, a German psychiatrist, made the first measurement of electrical activity from the human brain, and called it *Electroenkephalogram* (Berger, 1929; Swartz and Goldensohn, 1998).

2.1.1 The Origin of the EEG

An EEG measured from the scalp is the summation of microscopic ionic currents from the large populations of underlying cortical neurons. The so-called pyramidal neurons located mainly in the fifth layer of the cortex are considered to contribute the most to the EEG. Pyramidal neurons have long straight dendrites perpendicular to the surface of the cortex, and thus, neighboring cells have approximately parallel dendrites. These pyramidal dendrites receive a large number of synaptic connections from other neurons. When neighboring pyramidal neurons are activated synchronously, their individual current flows are summed, and as a result, a remarkably larger regional current flow is formed. This larger current flow generates voltage, which can be detected as the EEG on the scalp. An EEG measured at the scalp and generated by cortical neurons may originate from either the cortex itself or the subcortical structures which indirectly trigger the activity of cortical neurons (Rampil, 1998; Lukatch and Greenwald, 2003; Lipping and Jäntti, 2004).

2.1.2 Measurement of the EEG

A diagnostic EEG signal is most commonly measured using scalp electrodes located according to the 10–20 electrode placement system (Sharbrough *et al.*, 1991). The 10–20 system describes

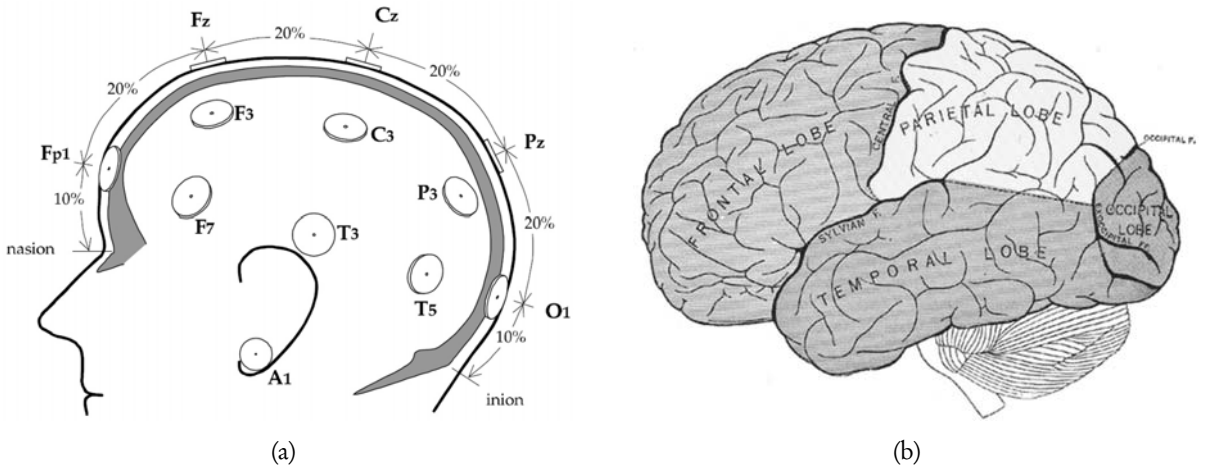

(a) (b)

Figure 2.1 — (a): illustration of the 10–20 EEG electrode location system (picture adapted from van de Velde (2000)). (b): location of the frontal, temporal, parietal, and occipital lobes of the human brain (picture adapted from Gray (2000)).

how electrodes are located on the scalp. The location of the electrodes on the front-back line is based on dividing the distance between the nasion and the inion over the vertex in the midline. There are five locations marked along that line: frontal polar "Fp", frontal "F", central "C", parietal "P", and occipital "O" (Fig. 2.1(a)). The first location, "Fp", is located at 10% of the nasion-inion distance, the second point, "F", at 20% of that distance from the point "Fp" and so on in 20% steps. Lastly, the distance between point "O" and the inion is again 10% of the whole distance.

The electrode names come from anatomical terms for the brain lobes (see Fig. 2.1(b)); however, the central region is an exception since there is no central lobe of the brain. In order to differentiate electrode locations between left and right hemispheres, even numbers are used as subscripts for the right hemisphere and odd numbers for the left hemisphere. The letter "z" stands for an electrode placed on the midline. If necessary, additional more closely spaced electrodes can be added (American Electroencephalographic Society, 1994; Jasper, 1958).

In contrast, when EEG monitoring is performed in the operating room or intensive care unit (ICU), often only a limited number of electrodes—2 or 4—are used (van Gils *et al.*, 2002; Smith *et al.*, 2006). In this case the electrodes are most often located on the forehead.

The EEG signal measured from the electrodes is filtered by pre-filters, which remove very low frequencies (usually below 0.5 Hz) and frequencies above the Nyquist limit. Removal of the very low frequencies is often necessary to avoid drift of the signal's baseline, while removal of the frequencies above the Nyquist limit is necessary to prevent aliasing. Removal of high frequencies depends on the application: it is common that 70 Hz is the upper limit for routine EEG recordings. In the case of some clinical tests or evoked potentials recording, much higher cutoff frequency may be needed. After analog prefiltering the EEG signal is amplified and digitized (Smith *et al.*, 2006).

Table 2.1 — Definition of the EEG rhythms according to the frequency content (Niedermayer, 1999).

EEG rhythm	Frequency range, Hz
Delta (δ)	< 4
Theta (θ)	4 – 7
Alpha (α)	8 – 13
Beta (β)	14 – 30
Gamma (γ)	> 30

2.1.3 Classification of the EEG

The EEG signal is classically divided into five different rhythms according to the frequency band of the signal. The rhythms and corresponding frequency bands are shown in Table 2.1. The proportion of these rhythms in a subject's EEG depends on his/her age and mental status.

The delta rhythm is typically seen during deep slow wave sleep, and it has relatively large amplitude. In addition, the delta rhythm can occur in the cases of brain injury and coma as well as during anesthesia. The theta rhythm can be seen during certain stages of sleep and in states of quiet focus such as during meditation (Aftanas and Golosheykin, 2005). The alpha rhythm dominates during periods of relaxation with eyes closed but still awake. The alpha rhythm has the largest amplitude in the occipital regions. Sometimes the alpha rhythm is also called "Berger's wave" in memory of the founder of the EEG. The beta rhythm is associated with normal waking consciousness states. Low amplitude beta rhythm is often connected with active thinking and concentration. In particular, rhythmic beta with a dominant frequency is associated with several pathologies and drug effects. The gamma rhythm of the brain is associated with perception and consciousness (Vanderwolf, 2000). It has been shown that gamma activity occurs during waking or active sleep as well as in a burst-suppression pattern in anesthesia (Vanderwolf, 2000).

2.2 Sedation and Anesthesia

The definitions of sedation and anesthesia are referring to the patients's level of awareness and response to stimulation. The term "sedation" comes from the Latin word *sedare*, meaning "to settle", "to calm" (Harper, 2001). The term "anesthesia" comes from the Greek word *anaisthesia*, meaning "lack of sensation", "loss of feeling" (Harper, 2001).

The term sedation is used when a patient in the ICU, for example, is given a small dose of anesthetic drug to make him/her calm and minimize anxiety. Sedation is sometimes further divided into two subcategories: light sedation and deep sedation. Light sedation is the state where the level of consciousness is minimally suppressed, and the patient is able to breathe independently and to respond appropriately to verbal command or physical stimulation. Deep

Table 2.2 — Responsiveness scores for the modified OAA/S scale.

Score	Responsiveness
5	Responds readily to name spoken in normal tone
4	Lethargic response to name spoken in normal tone
3	Responds only after name is called loudly or repeatedly
2	Responds only after mild prodding or shaking
1	Responds only after painful trapezius squeeze
0	No response after painful trapezius squeeze

sedation, on the other hand, is defined as the state of moderately suppressed consciousness or the state of unconsciousness. The patient is not easily aroused from deep sedation and the protective reflexes, i.e. independent breathing and responses to verbal or physical stimuli, are not preserved (Murphy, 1996).

The depth of sedation can be clinically assessed, for example, by using the Ramsay score or the Observer's Assessment of Alertness/Sedation (OAA/S) score (Ramsay *et al.*, 1974; Chernik *et al.*, 1990; Glass *et al.*, 1997). The responsiveness scores for the modified OAA/S scale are shown in Table 2.2 (Glass *et al.*, 1997).

Anesthesia is defined as the state of unconsciousness, amnesia, and hemodynamic, motor, and endocrinologic stability during surgery, produced by specific medication (van Gils *et al.*, 2002). This means that for achieving an adequate level of anesthesia, usually a combination of hypnotics, analgesics, and neuromuscular blocking agents are used. Therefore, general anesthesia consists of three partially dependent components: a) hypnosis, b) analgesia, and c) muscle relaxation. A short description of each of these components is given subsequently.

Hypnosis With the use of hypnotic medication the patient is taken to the unconscious state, i.e. he/she is unaware of ongoing events (surgical procedures, for example). In addition, hypnosis has to assure amnesia, i.e. the patient should not remember anything that happened during the operation.

Analgesia Analgesia (i.e. painlessness) is obtained with the use of analgesic medication. Despite the fact that the patient could be in deep hypnosis, his/her body can still perceive the pain. That kind of situation is called nociception. Therefore, the purpose of analgesia is to assure antinociception, i.e. patient's body should not perceive any pain during surgical operation.

Muscle relaxation The relaxed state of muscles is often required for the surgeon to perform an operation. Muscle relaxation is usually obtained either by the use of neuromuscular blocking agents or sufficient combination of hypnosis and analgesia.

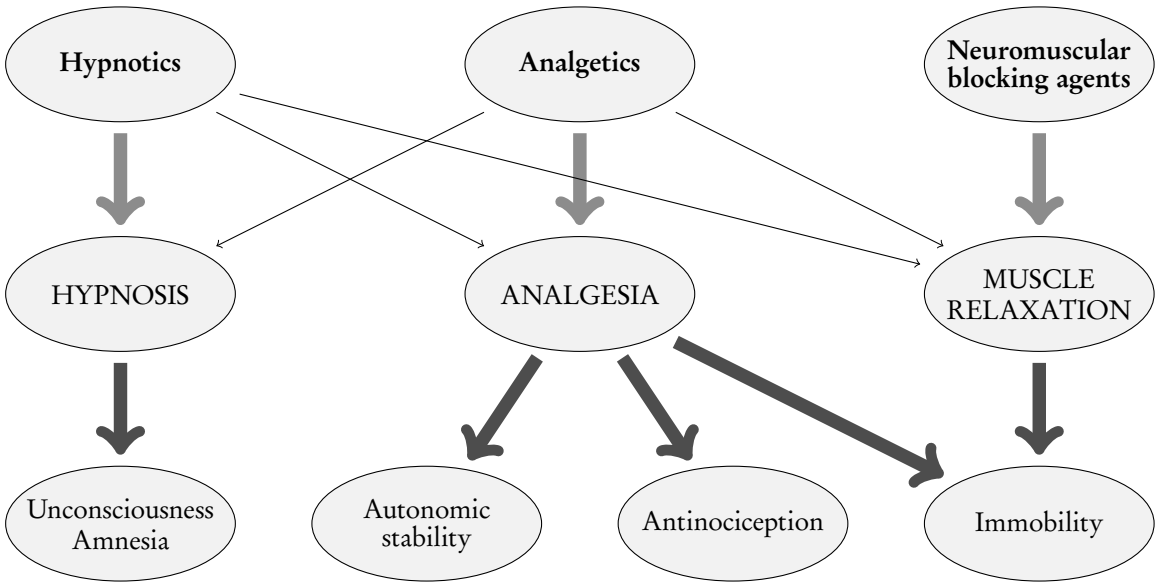

Figure 2.2 — Scheme of nonlinear drug-effect relationship. Diagram adapted from van Gils *et al.* (2002).

Murphy (1996) has stated that a patient is adequately anesthetized when awareness is suppressed completely, incision does not produce movement, and the patient's responses to surgical stimulation are eliminated or minimal.

Fig. 2.2 shows that the relationship between drugs (hypnotics, analgetics, and neuromuscular blocking agents) and desired responses (hypnosis, analgesia, and muscle relaxation) is not a simple one-to-one connection. Instead, these relationships are complex and definitely nonlinear.

2.3 EEG Signal during Anesthesia

Anesthetic drugs influence both the frequency content and the amplitude of the EEG signal. Despite the fact that each drug has specific dose-related EEG effects, they all share some common characteristics. In Table 2.3 the EEG effects of drugs called sevoflurane and propofol are compared. For both intravenous and inhaled anesthetics, subanesthetic doses usually cause an increase in frontal beta activity and suppression of alpha activity that normally can be seen in the occipital region. Thereafter, EEG turns into large-amplitude, slow-wave activity with superimposed widespread alpha activity. Further increasing the dose of the anesthetic drug causes the slow activity to increase until short flat periods of EEG—the so-called suppression—appear. The duration of suppression periods increases gradually, and the high amplitude activity periods—the so-called bursts—shorten (subsection 2.3.1). If the doses are further increased, the occurrence of the bursts gradually decreases until they disappear, and the EEG is continuously in suppression.

Table 2.3 — The effect of sevoflurane (inhaled) and propofol (intravenous) anesthesia on EEG signal characteristics. Table adapted from Miller (2000).

Anesthetic drug	Anesthetic level	Effect on EEG frequency
Sevoflurane	Subanesthetic	Loss of alpha Frontal beta
	Anesthetic	Frontal 4–8 Hz activity
	Increasing dose	Diffuse theta and delta Burst-suppression Silence
Propofol	Low dose	Loss of alpha Frontal beta
	Moderate dose	Frontal delta Waxing/waning alpha
	Increasing high dose	Diffuse delta Burst-suppression Silence

2.3.1 Burst-Suppression Pattern

Burst-suppression (BS) is the signal pattern where large-amplitude, mixed-activity bursts followed by significantly suppressed activity periods are occurring repeatedly. The BS pattern can occur, for example, during ischemia, very strong hypothermia, and deep surgical anesthesia (Smith *et al.*, 2006). The BS pattern represents abnormal cortical activity during which about 95% of the cortical cells are inactive (Steriade *et al.*, 1994). Therefore, it can be concluded that during BS the patient is in a deeply unconscious state. More importantly, the BS pattern in a healthy patient can be produced only by large concentrations of an anesthetic drug (Hoffman and Edelman, 1995; Huotari *et al.*, 2004). It is also known that different anesthetic drugs produce different BS patterns, suggesting that their action mechanisms are different (Watts *et al.*, 1999; Huotari *et al.*, 2004).

Examples of typical EEG patterns during anesthesia at the BS level in propofol and sevoflurane anesthesia are shown in Fig. 2.3. By inspecting Fig. 2.3 visually, one can notice that in comparison with the burst induced by propofol, the sevoflurane burst has a more complex structure. Bursts induced by sevoflurane tend to contain a higher proportion of large-amplitude, abrupt activity while propofol bursts mainly contain slow wave activity with superimposed mixed higher frequency activity. In addition, the spindle activity (subsection 2.3.2) can occur during anesthesia induced by propofol.

2.3.2 EEG Spindles

The spindle is a specific EEG pattern appearing during sleep. Spindles are defined as 1–3 second periods of waxing and waning 7–14 Hz oscillations usually superimposed on top of the other

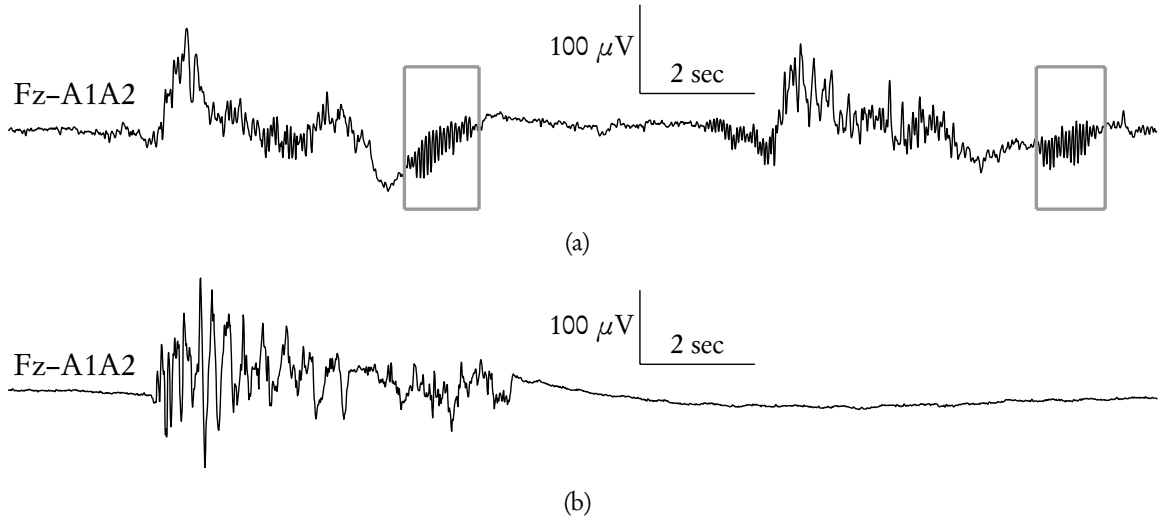

Figure 2.3 — Example of a typical BS pattern during deep anesthesia induced by propofol (a) and sevoflurane (b). Gray boxes denote spindle patterns, which can occur during propofol anesthesia. For both cases the surface electrode Fz with the reference at joint A1A2 lead is used.

EEG activity (McCormick and Bal, 1997; Amzica and Steriade, 1995). Spindle oscillation is generated as a result of interaction between thalamocortical and thalamic reticular cells (Bazhenov *et al.*, 2000; Steriade and Timofeev, 2003). Additionally, spindles have been studied during normal physiological sleep in order to examine sleep stages and sleep disorders (Himanen *et al.*, 2002, 2003). The results of these studies showed that spindle frequencies were slower for sleep apnea patients than for the healthy patients. The authors conclude that lower sleep spindle frequency could indicate disturbed sleep and altered neural mechanisms regulating sleep.

In addition to physiological sleep, spindle patterns can occur during deep anesthesia induced by propofol (Jäntti *et al.*, 1993; Huotari *et al.*, 2004; Wolter *et al.*, 2006). Spindle patterns induced by propofol can be most clearly seen during deep anesthesia when the BS pattern already is "turned on". The frequency of the spindles is usually in the range of 13–15 Hz and the duration roughly in the range of 2–5 seconds (Huotari *et al.*, 2004). Usually, spindles occur after the burst but sometimes they can occur during longer suppression periods or during bursts as well. Fig. 2.3(a) illustrates a typical situation when bursts are followed by spindles during deep propofol anesthesia.

It has been shown that synchronous EEG activity corresponding to spindles can, in fact, be detected even before the BS starts. At the beginning this activity has the frequency of about 20 Hz, which thereafter, as anesthesia deepens, gradually decreases down to about 13 Hz as BS starts (publication **VI**).

Several methods have been used for analyzing (sleep) spindles. For example, Durka *et al.* (2005) have applied a method called matching pursuit (Mallat and Zhang, 1993; Mallat, 1999) to sleep spindles in order to obtain high resolution results. A through and comprehensive overview of the analysis of EEG spindles is given by Żygierewicz (2000).

CHAPTER **3**

Regularity Analysis of the EEG signal

This chapter gives an overview of the regularity/complexity measures used in this thesis for analyzing the EEG signal. The main emphasis is on the following regularity/complexity measures: Shannon entropy (publication **III**), spectral entropy (publications **II**, **III**, **IV**, and **V**), approximate entropy (publications **II**, **III**, **IV**, and **V**), Lempel-Ziv complexity (publications **II**, **III**, **IV**, and **V**), and Higuchi fractal dimension (publications **II**, **III**, **IV**, and **V**).

It has been argued that besides the EEG phase synchrony, a sufficient complexity of brain dynamics is essential for conscious brain activity (Tononi and Edelman, 1998). In their dynamical model Tononi and Edelman emphasize that synchronized brain activity is a necessary but not a sufficient condition for conscious brain functioning. The authors hypothesize that at least another factor—*complexity*—is important in order to guarantee a sufficient differentiation of brain dynamics. In addition, Fell *et al.* (2003) propose that *chaoticity* of the EEG may be another necessary condition for conscious brain functioning. Despite the fact that the evidence for chaotic brain dynamics is controversial and inconclusive, the chaoticity in brain dynamics may explain the flexibility and fast reactivity of the brain (Fell *et al.*, 2003).

3.1 Measures for Estimating Signal Regularity/Complexity

There are several methods used for estimating regularity/complexity properties of the signal. Many of these are so-called entropy based methods, i.e. they are based on estimating a certain type of entropy of the signal. Since the term "entropy" is used in different fields—for example, in physics, information theory, and signal processing—it can cause misunderstandings. In order to explain how the term "entropy" has been used over the course of time, a brief history of entropy is given in Appendix A.

The classic method for estimating regularity of a signal is *Shannon entropy* (ShEn). A detailed description of ShEn is given in subsection 3.1.1. Another regularity measure widely used in EEG analysis—*spectral entropy* (SpEn)—is overviewed in subsection 3.1.2. The third entropy-based measure in this thesis is *approximate entropy* (ApEn), which is described in subsection 3.1.3. Subsection 3.1.4 gives an overview of a coarse-grained complexity measure called Lempel-Ziv complexity (LZC), and finally, in subsection 3.1.5 an overview of a fractal dimension estimator—Higuchi fractal dimension (HFD)—is given.

3.1.1 Shannon Entropy

The concept of entropy in the context of information theory was introduced by Shannon (1948), and it can be viewed as a measure of order in the signal. Shannon entropy of a discrete signal is defined as

$$H_{Sh} = -\sum_{i=1}^{N_a} p_i \log p_i, \tag{3.1}$$

where N_a is the number of all possible amplitude values in the signal and p_i is the probability that the amplitude a_i is one of these values.

In general, it is not reasonable to take into account all amplitude values. Instead, signal amplitude values are divided into bins, i.e. the probability density function (PDF) of the signal is estimated by means of a histogram. In this case N_a corresponds to the number of bins in the histogram.

In order to obtain a normalized value for Shannon entropy, H_{Sh}, Eq. 3.1 should be modified as follows:

$$\mathrm{ShEn} = \frac{H_{Sh}}{\log N_a}. \tag{3.2}$$

By using Eq. 3.1 it can be shown that a signal with a sharp PDF has small H_{Sh} value, whereas, a signal with a flat PDF has a larger H_{Sh}. Let us assume that a discrete random variable has two possible amplitude values, and let p_1 and p_2 denote the probability that it takes value 1 or 2, respectively. Then, if $p_1 \gg p_2$, i.e. the signal takes mostly only one value (PDF is sharp), Eq. 3.1 yields a small value. On the other hand, if $p_1 \approx p_2$, i.e. signal values are almost equiprobable (PDF is flat), then a much larger value is obtained by applying Eq. 3.1. For example, if $p_1 = 0.99$ and $p_2 = 0.01$ then Eq. 3.1 yields that $H_{Sh} = 0.056$, while for $p_1 = p_2 = 0.5$ the result would be $H_{Sh} = 0.693$.[1]

The main difficulty related to the calculation of ShEn is the estimation of the signal PDF (Bercher and Vignat, 2000). In fact, the problem is more general and must be faced everywhere where estimation of PDF is involved (for example, Pham (1996, 2004)).

3.1.2 Spectral entropy

Spectral entropy, introduced by Powell and Percival (1979) and further developed by Inouye *et al.* (1991), is based on Shannon entropy (3.1), where the PDF of a signal is replaced by its power spectrum, P. Spectral entropy is defined as

$$H_{Sp} = -\sum_{i=f_{low}}^{f_{high}} P_i \log P_i, \tag{3.3}$$

[1]The calculations presented here are performed by using the natural logarithm. If the base of logarithm was 2, then the corresponding entropies would be $H_{Sh} = 0.08$ and $H_{Sh} = 1$, respectively.

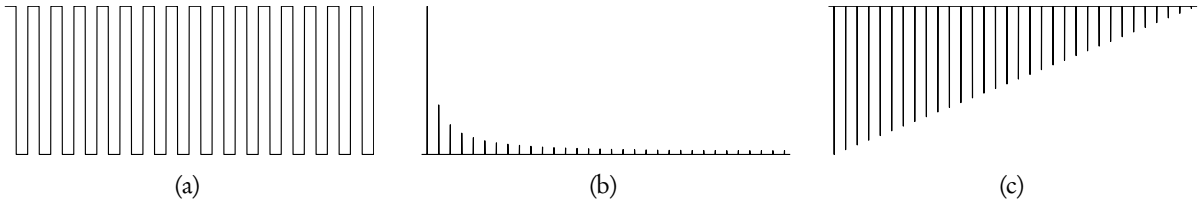

Figure 3.1 — Rectangular signal (a), the magnitude (b), and phase of its Fourier' transform. The frequency range of the x-axis for plots (b) and (c) is from 0 to the Nyquist frequency.

where f_{low} and f_{high} are the lowest and highest frequencies in the spectrum, respectively, used for the H_{Sp} calculation. In addition, before applying Eq. 3.3, the power spectrum P has to be normalized so that the condition

$$\sum_i P_i = 1 \tag{3.4}$$

would be fulfilled (Inouye *et al.*, 1991; Viertiö-Oja *et al.*, 2004; Rezek and Roberts, 1998; Vakkuri *et al.*, 2004). Usually spectral entropy is normalized as well as

$$\mathrm{SpEn} = \frac{H_{Sp}}{\log N_f}, \tag{3.5}$$

where N_f is the number of frequency components in the frequency range $[f_{low}, f_{high}]$.

It follows from Eq. 3.5 that signals having sharp or "spiky" power spectra have low SpEn. A flat power spectrum, on the other hand, gives a high value for SpEn. The reasoning here is the same as for ShEn (subsection 3.1.1); the only difference is that now the probabilities of the signal amplitude values are replaced by the values of its power spectrum.

Eq. 3.3 shows that the calculation of SpEn takes into account only the power spectrum of the signal while all phase information is discarded. Thus, by randomizing the phase it is possible to create an arbitrary number of signals having the same power spectrum and, therefore, the same SpEn values. This phenomenon can be shown by taking a rectangular signal, for instance, and calculating its magnitude and phase spectrums by means of the Fourier transform. The results for a rectangular signal are presented in Fig. 3.1. Thereafter, by replacing the phases with random numbers (i.e. by randomizing them) and taking the inverse Fourier transform, a signal having the same power spectrum as the original signal is obtained. Examples of such signals are given in Fig. 3.2. It can be seen that the signals in Fig. 3.2 show more complex structure than the original rectangular signal. Although the first component of the magnitude spectrum (Fig. 3.1(b)) is significantly larger than the other higher components, all the signals in Fig. 3.2 have the same fundamental frequency as the original rectangular signal.

Another property of SpEn is that it does not take into account the order of the frequency components in the power spectrum. This, in turn, allows the creation of an arbitrary number of signals by randomizing the order of the frequency components in the power spectrum while still having the same SpEn values. Fig. 3.3 gives an example of signals having power spectra obtained by randomizing the order of the frequency components of the spectrum of the rectangular signal (original phases are preserved). By comparison with the signals in Fig. 3.2, the

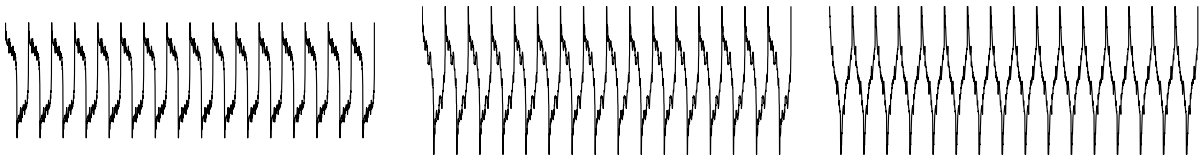

Figure 3.2 — Examples of signals having the same power spectrum as the signal in Fig. 3.1(a). The phases from Fig. 3.1(c) have been replaced by random numbers in the range $-\pi \ldots \pi$.

Figure 3.3 — Examples of signals having the same spectral components as the signal in Fig. 3.1(a). The order of the frequency components (Fig. 3.1(b)) has been randomized. Original phases have been preserved.

signals in Fig. 3.3 show even more complex structure since the large fundamental component of the rectangular signal is not necessarily preserved anymore.

3.1.3 Approximate entropy

Approximate entropy (ApEn), introduced by Pincus *et al.* (1991), is a measure quantifying the regularity of the signal. ApEn is an approximation of the Kolmogorov-Sinai (KS) entropy by adapting it to signals of finite length.

The algorithm of ApEn for a discrete signal s of finite length N begins by fixing a positive integer m and a positive real number r. Parameters m and r correspond to the vector length (it is also called the embedding dimension of the phase space) and maximum allowable distance between two vectors (distance between two phase-space points), respectively.[2] Thereafter, $N - m + 1$ vectors $\mathbf{x}_m(i) = \{s(i), s(i+1), \ldots, s(i+m-1)\}$ are formed from the signal s. Next, for each i, $1 \leqslant i \leqslant N - m + 1$, the quantity $C_i^m(r)$ is calculated as follows:

$$C_i^m(r) = \frac{\text{number of } j \text{ such that } d[\mathbf{x}_m(i), \mathbf{x}_m(j)] \leqslant r}{N - m + 1}, \tag{3.6}$$

where d denotes the distance between two vectors $\mathbf{x}_m(i)$ and $\mathbf{x}_m(j)$. Often, the distance d is calculated by using a maximum norm:

$$d[\mathbf{x}_m(i), \mathbf{x}_m(j)] = \max_{k=1,\ldots,m} (|s(i+k-1) - s(j+k-1)|). \tag{3.7}$$

[2] A brief explanation of the phase-space concept is given in Appendix B.

The quantity $C_i^m(r)$ is the probability that any vector $\mathbf{x}_m(j)$ is within the distance r of $\mathbf{x}_m(i)$. Based on Eq. 3.6, the average of the logarithms of the functions, $C_i^m(r)$ and $\Phi^m(r)$, is defined as:

$$\Phi^m(r) = \frac{1}{N-m+1} \sum_{i=1}^{N-m+1} \log C_i^m(r). \tag{3.8}$$

KS entropy is defined by using Eq. 3.8 as follows (Eckmann and Ruelle, 1985; Pincus *et al.*, 1991):

$$\text{KS entropy} = \lim_{r\to 0} \lim_{m\to\infty} \lim_{N\to\infty} [\Phi^m(r) - \Phi^{m+1}(r)]. \tag{3.9}$$

Due to the limits in Eq. 3.9, this definition is not suitable for the analysis of finite and noisy signals obtained from measurements (Pincus *et al.*, 1991; Richman and Moorman, 2000).

Pincus (1991) defined ApEn for fixed parameters m and r as a family of formulas:

$$\text{ApEn}(m,r) = \lim_{N\to\infty} [\Phi^m(r) - \Phi^{m+1}(r)], \tag{3.10}$$

which for finite length signals is estimated by the following family of statistics:

$$\text{ApEn}(m,r,N) = \Phi^m(r) - \Phi^{m+1}(r). \tag{3.11}$$

By using conditional probabilities, it is possible to give Eq. 3.11 the following interpretation (Pincus *et al.*, 1991):

$$\begin{aligned} -\text{ApEn} &= \Phi^{m+1}(r) - \Phi^m(r) \\ &= \text{ average over } i \text{ of } \log[\text{conditional probability that} \\ &\quad |s(j+m) - s(i+m)| \leqslant r, \text{ given that} \\ &\quad |s(j+k) - s(i+k)| \leqslant r \text{ for } k = 0,1,\ldots,m-1]. \end{aligned} \tag{3.12}$$

ApEn can be thought of as the negative logarithm of the probability, where points that are close in m-dimensional space remain close in $m+1$-dimensional space. In addition, it can be shown that the upper bound for ApEn is given by the following relation (Richman and Moorman, 2000): $\text{ApEn}(m,r,N) \leqslant \log(N-m)$.

In order to obtain accurate estimates for conditional probabilities described in Eq. 3.12 the length of the signal should be at least 10^m and preferably 20^m to 30^m data points (Pincus *et al.*, 1991; Pincus and Goldberger, 1994). Consequently, this sets practical limits for selecting values for m. In addition, it has been suggested that the parameter r should be in the range of 10–25% of the signal standard deviation (Pincus *et al.*, 1991; Pincus and Goldberger, 1994).

When applying ApEn calculations to the measured signals, it must be kept in mind that ApEn suffers from the bias effect and that it is strongly dependent on the length of the signal (Pincus, 1991; Pincus *et al.*, 1991). In addition, Richman and Moorman (2000) show that in some cases ApEn lacks consistency.

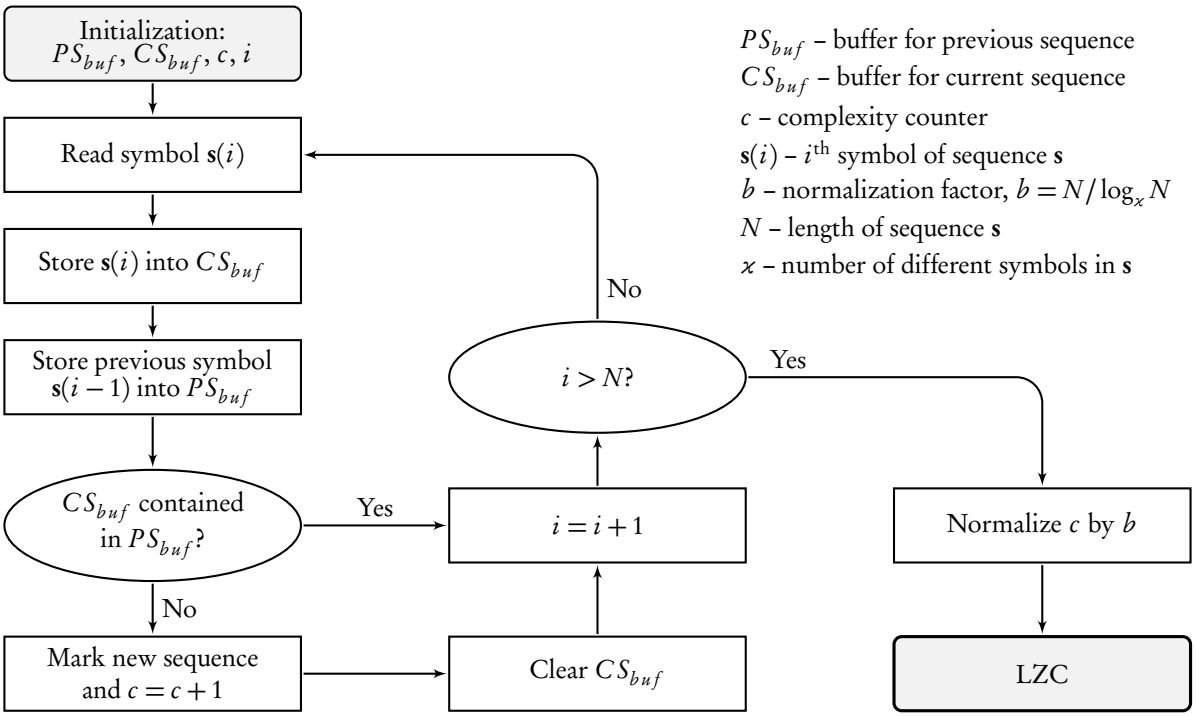

Figure 3.4 — Block diagram of the algorithm for calculating Lempel-Ziv complexity of the sequence of symbols **s**. Diagram adapted from Zhang *et al.* (2001).

3.1.4 Lempel-Ziv Complexity

Lempel-Ziv complexity (LZC) introduced by Lempel and Ziv (1976) is a measure expressing the rate of a new subsequence (pattern) generation along the given sequence of symbols **s**. The procedure for calculating LZC is illustrated in Fig. 3.4. The idea behind the calculation of LZC is the following: the algorithm goes through the sequence of symbols **s** counting different subsequences found in **s**. Every time a new subsequence is found, the complexity counter c is increased by 1, and finally, the result is normalized:

$$\mathrm{LZC} = \frac{c}{b}, \tag{3.13}$$

where b is the normalization factor defined as

$$b = \frac{N}{\log_{\varkappa} N}. \tag{3.14}$$

In Eq. 3.14, N denotes the length of the sequence **s**, and $\varkappa$ is the number of different symbols in **s**.

Therefore, a sequence consisting of many similar subsequences (patterns) has a low LZC value (low complexity), while a sequence containing a large number of different subsequences has a high LZC value (high complexity).

For instance, in the following binary sequence of 18 symbols, $\mathbf{s} = 101001010010111110$, there are 8 different subsequences: 1|0|10|01|010|0101|11|110 (vertical line | denotes the separation between different subsequences). Since $\mathbf{s}$ is a binary sequence, the number of different symbols, $\varkappa$, is 2, and therefore, by applying Eq. 3.13, we obtain: $\mathrm{LZC} = 8/(18/\log_2 18) \approx 1.85$.

Prior to applying the LZC algorithm, the signal s has to be converted into the sequence of symbols $\mathbf{s}$. If $\varkappa = 2$, i.e. there are two different symbols in $\mathbf{s}$, the conversion can be done as follows:

$$\mathbf{s}(i) = \begin{cases} 0 & \text{if } s(i) < T_d \\ 1 & \text{if } s(i) \geqslant T_d \end{cases}, \tag{3.15}$$

where $\mathbf{s}(i)$ and $s(i)$ are the current symbol and the current sample in $\mathbf{s}$ and s, respectively. T_d denotes the threshold, which can be calculated as $T_d = \mathrm{mean}\{s\}$ (Zhang *et al.*, 2001) or $T_d = \mathrm{median}\{s\}$ (Abásolo *et al.*, 2006b).

Several authors have stated that it is sufficient to use $\varkappa = 2$ for practical calculations (Xu *et al.*, 1997; Radhakrishnan and Gangadhar, 1998; Zhang *et al.*, 2001; Szczepański *et al.*, 2003); however Abásolo *et al.* (2006b) suggest using $\varkappa = 3$ since more information is preserved during the conversion process.

3.1.5 Higuchi Fractal Dimension

In 1988 Higuchi introduced an algorithm for estimating a signal fractal dimension[3] directly in the time domain.

Estimating a fractal dimension according to the Higuchi algorithm is based on the following scheme. From the given signal $s = \{s(1), s(2), \ldots, s(N)\}$, k new curves s_j^k are constructed as follows:

$$s_j^k = \left\{ s(j), s(j+k), s(j+2k), \ldots, s\left(j + \left\lfloor \frac{N-j}{k} \right\rfloor k\right) \right\} \quad j = 1, 2, \ldots, k, \tag{3.16}$$

where both j and k are integers and $\lfloor \cdot \rfloor$ denotes the floor operation. j denotes the initial time and k is the time interval between samples. N denotes the length of the signal s. Then the length $L_j(k)$ for each constructed curve s_j^k is calculated as

$$L_j(k) = \frac{1}{k} \left[\left(\sum_{i=1}^{\lfloor \frac{N-j}{k} \rfloor} |s(j+ik) - s(j+(i-1)k)| \right) \cdot \frac{N-1}{\lfloor \frac{N-j}{k} \rfloor k} \right]. \tag{3.17}$$

The length $L_j(k)$ is calculated for all curves having the same time interval k for $j = 1, ..., k$.

This procedure is repeated for each k ranging from 1 to $k_{\max}$, and then for each k, the average length is calculated as

$$L(k) = \frac{1}{k} \sum_{j=1}^{k} L_j(k). \tag{3.18}$$

[3] The concept of a fractal dimension is briefly described in Appendix B.

The curve length calculation procedure for the case $k = 3$ and j having the values $j = 1, 2, 3$ is illustrated in Fig. 3.5. The bold vertical lines in Fig. 3.5 denote the difference between sample values being k samples apart, i.e. $|s(j + ik) - s(j + (i - 1)k)|$, which are summed up and normalized, as defined by Eq. 3.17. Thereafter, the individual lengths $L_j(k)$ are averaged according to Eq. 3.18, and the average curve length, $L(k)$, for given k is obtained.

If the relation $L(k) \propto k^{-D}$ approximately holds, then the signal s can be considered as fractal-like with the dimension D. Therefore, when $L(k)$ is plotted against $1/k$, where $k = 1, ..., k_{\max}$, in a double-logarithmic plot, the data points should fall into a straight line with the slope D. The estimate of the fractal dimension D is the slope of the least-squares linear fit applied to the pairs $(\log 1/k,\ \log L(k))$, where $k = 1, ..., k_{\max}$.

It has been claimed that the main advantage of the Higuchi algorithm over the "conventional" correlation-dimension algorithm is its speed since there is no need for reconstructing the attractor in the phase-space (Esteller *et al.*, 1999, 2001; Bashashati *et al.*, 2003).

3.2 Literature Overview Related to the Regularity/Complexity Analysis of the EEG Signal

The regularity and complexity measures described in subsections 3.1.1–3.1.5 have been widely applied to the analysis of the EEG signal measured in various situations like anesthesia and/or sedation, Alzheimer's disease, hypothermia, ischemia, and epilepsy. In addition, they have been also quite popular for analyzing several cardiovascular diseases. Subsequently a short overview of the literature related to EEG complexity analysis is given.

Shannon entropy ShEn is used to study the effects of desflurane on the EEG signal (Bruhn *et al.*, 2001b). Bruhn *et al.* (2002) note the usefulness of ShEn since it is highly robust against several artifacts occurring in the EEG signal. Thakor *et al.* (2006) and Shin *et al.* (2006) have applied ShEn to the EEG in order to study the effect of hypothermia on neurological recovery of the brain after cardiac arrest. Based on ShEn, they have derived a new measure called information quantity. The authors report that both measures have a good capability to track changes in the EEG during hypothermia. Bezerianos *et al.* (2003) have used ShEn and Tsallis entropy (see Appendix A for more details about Tsallis entropy) to detect brain injury level caused by ischemia. The authors conclude that both measures are able to describe in a satisfactory manner the changes in the EEG that occur after ischemic insult.

Spectral Entropy The first application of SpEn in the EEG analysis was to quantify regularity of the alpha rhythm, i.e. to measure wakefulness rather than the unconsciousness (Inouye *et al.*, 1991). SpEn also is used for monitoring the depth of anesthesia (Rezek and Roberts, 1998; Zhang and Roy, 2001; Ellerkmann *et al.*, 2004; Vakkuri *et al.*, 2005; Maksimow *et al.*, 2006). Additionally, the algorithm of SpEn has been implemented and used in the Entropy module of the commercially available anesthesia monitor S/5$^{\text{TM}}$ by GE Healthcare Finland OY, the former Datex-Ohmeda (Viertiö-Oja *et al.*, 2004; Vakkuri *et al.*, 2004). It has been shown that SpEn decreases suddenly as the patient becomes unconscious during the induction of anesthesia, and

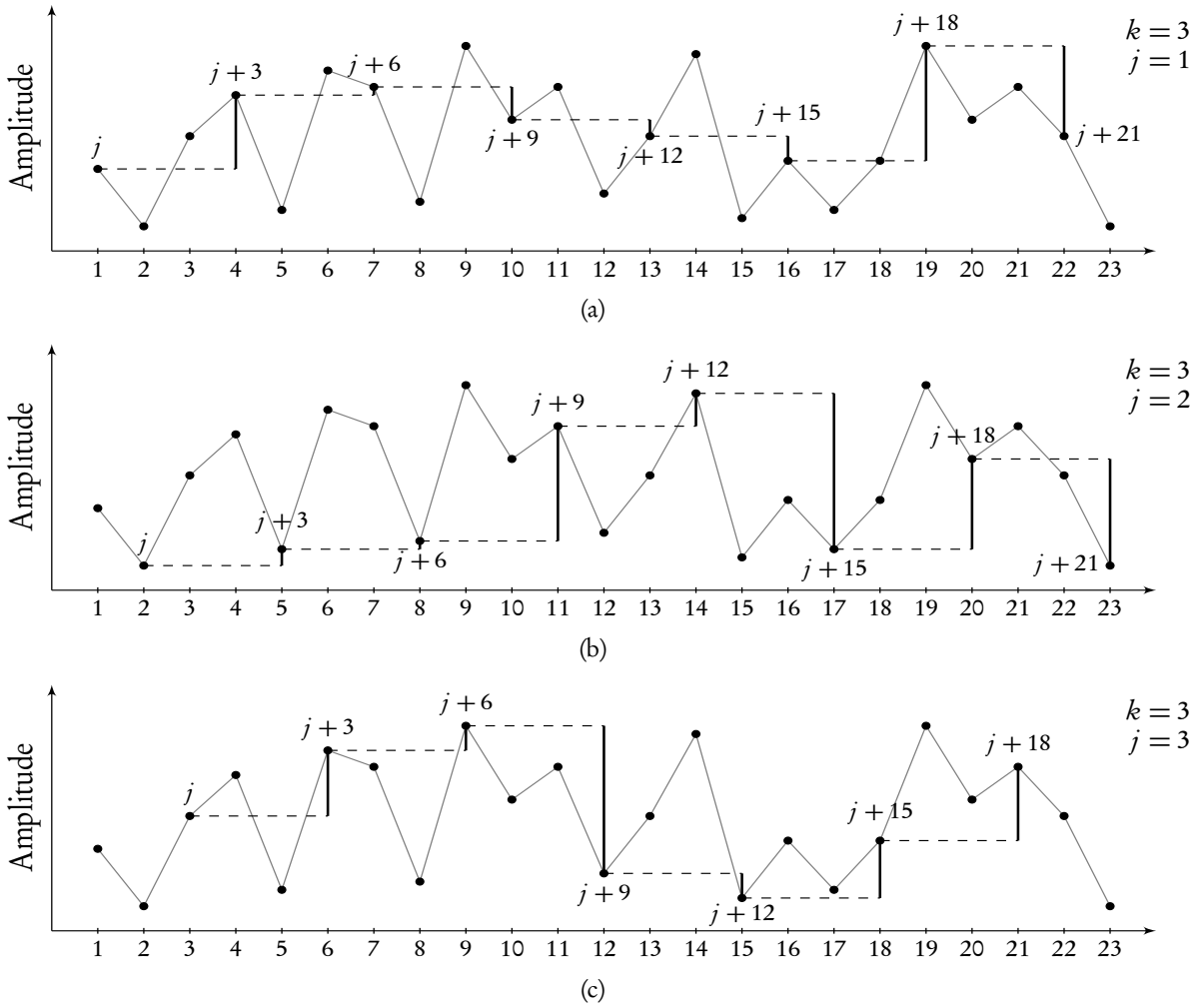

Figure 3.5 — An example of calculating the curve length $L_j(k)$, when the time interval is 3, i.e. $k = 3$, and the initial time, j, is taking values $j = 1$ (a), $j = 2$ (b), and $j = 3$ (c). The bold vertical lines denote the difference between sample values being k samples apart.

it does not decrease significantly with further deepening of the anesthesia (Sleigh *et al.*, 2004). In addition, Abásolo *et al.* (2006a) have used SpEn for analyzing EEG signals from patients having Alzheimer's disease. The authors reported that they did not find significant differences between Alzheimer's disease patients and control subjects' EEGs with SpEn.

Approximate Entropy ApEn is a popular tool for analyzing drug effects of several anesthetics like desflurane (Bruhn *et al.*, 2000b, 2001b), isoflurane (Bruhn *et al.*, 2000c), and propofol (Bruhn *et al.*, 2001a, 2002, 2003; Bouillon *et al.*, 2004; Koskinen *et al.*, 2006). ApEn has also been used for analyzing EEG during physiological sleep (Burioka *et al.*, 2002, 2003, 2005b) as well as in the case of epilepsy (Burioka *et al.*, 2005a) and schizophrenia (Abásolo *et al.*, 2005). Additionally, ApEn has been widely applied in clinical cardiovascular studies—publications by Pincus *et al.* (1991); Goldberger *et al.* (1994); Ho *et al.* (1997); Mäkikallio *et al.* (1997); Ferrario

et al. (2006) are only a few examples.

Lempel-Ziv Complexity LZC has been used for analyzing changes in the EEG signal during anesthesia (Zhang and Roy, 1999; Zhang *et al.*, 2001; Jordan *et al.*, 2006). It has also been used for analyzing the EEG from the Alzheimer's disease patients (Abásolo *et al.*, 2006b) and schizophrenia patients (Hornero *et al.*, 2006). In addition, LZC has been applied to the analysis of the EEG during hypoxia (Jernajczyk *et al.*, 2006).

Higuchi Fractal Dimension HFD has been used for the assessment of the depth of sedation in the intensive care unit (Anier *et al.*, 2004). Additionally, HFD has been used for analyzing EEG from normal awake patients (Accardo *et al.*, 1997) and from epileptic patients (Arle and Simon, 1990; Accardo *et al.*, 1997). It has also been used for detecting the influence of the magnetic field (Klonowski *et al.*, 2000) as well as microwave stimulation on the EEG (Parts *et al.*, 2003) and in EEG-based-biofeedback systems (Bashashati *et al.*, 2003).

3.3 EEG Regularity/Complexity during Propofol Induced Sedation

In this section an overview of the behavior of regularity/complexity measures (described in subsections 3.1.2–3.1.5) during propofol induced sedation is given. This overview is mainly based on publication **V**; the detailed description of the whole study can be found therein.

In brief, 15 patients were sedated using propofol. The sedation was performed according to the step-wise protocol, where the propofol concentration was increased by small steps every 4 minutes. Shortly before each administration of increased propofol concentration the OAA/S score was assessed. Recorded EEG signals were visually inspected, and artifact removal was done manually. Thereafter, the EEG was segmented into 15 second segments, and SpEn, ApEn, LZC, and HFD were calculated for each segment.

Fig. 3.6 gives an example of the EEG-signal segments for different OAA/S scores (left column) and the corresponding power spectra (right column). In spite of the fact that the figure shows the EEG signals and power spectra from a single study, the phenomenon is more general and can be seen almost everywhere where propofol sedation is used. The figure illustrates rather clearly how the amplitude of the EEG gradually increases as the OAA/S score decreases, i.e. sedation deepens. Additionally, as the sedation deepens, the power spectrum of the EEG becomes more concentrated (i.e. a more emphasized spike appears in the spectrum) and it gradually shifts towards the lower frequencies.

Before applying the methods listed above, the EEG signal was filtered using two bandpass filters: a) 2–47 Hz and b) 2–32 Hz. The results of regularity/complexity calculations are shown in Fig. 3.7. The results show that in general the regularity/complexity of the EEG tends to decrease as time goes by, i.e. the concentration of propofol increases. This trend is especially clear for ApEn and HFD for the 2–47 Hz bandpass-filtered signal. Whereas the SpEn and LZC show a plateau phase or even slight increase for the same filter during the first 12 minutes. This kind of so-called biphasic effect becomes more emphasized when the EEG is filtered with a 2–32 Hz filter, i.e. higher frequencies are removed from the signal.

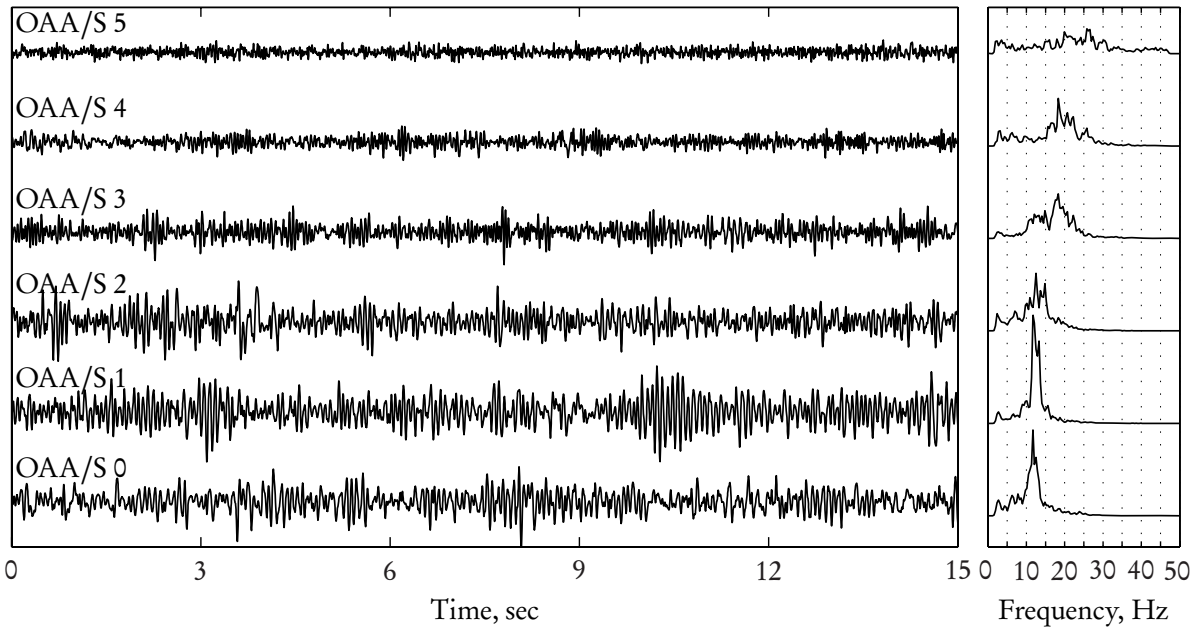

Figure 3.6 — Samples of 15 sec signal segments at different OAA/S levels (left column) and the corresponding power spectra (right column). All signals were filtered beforehand using a 2–47 Hz bandpass filter. The y-axis is in the same scale for all EEG signals and all power spectra are normalized according to Eq. 3.4.

Fig. 3.7 also illustrates how the assessment of the OAA/S score influences the behavior of the regularity/complexity measures. Namely, after every 4 minutes when the OAA/S score has been assessed, the values of the regularity/complexity measures undergo a sudden increase or jump. This effect is especially clear for the ApEn and HFD when the 2–47 Hz filter has been applied. The removal of the higher frequencies from the raw EEG signal tends to decrease that "jumping" effect. This kind of behavior is caused by the fact that stimuli accompanying the assessment of the OAA/S score actually influences the patient by bringing him/her into a lighter level of sedation. This phenomenon is described in more detail by Jensen *et al.* (2004).

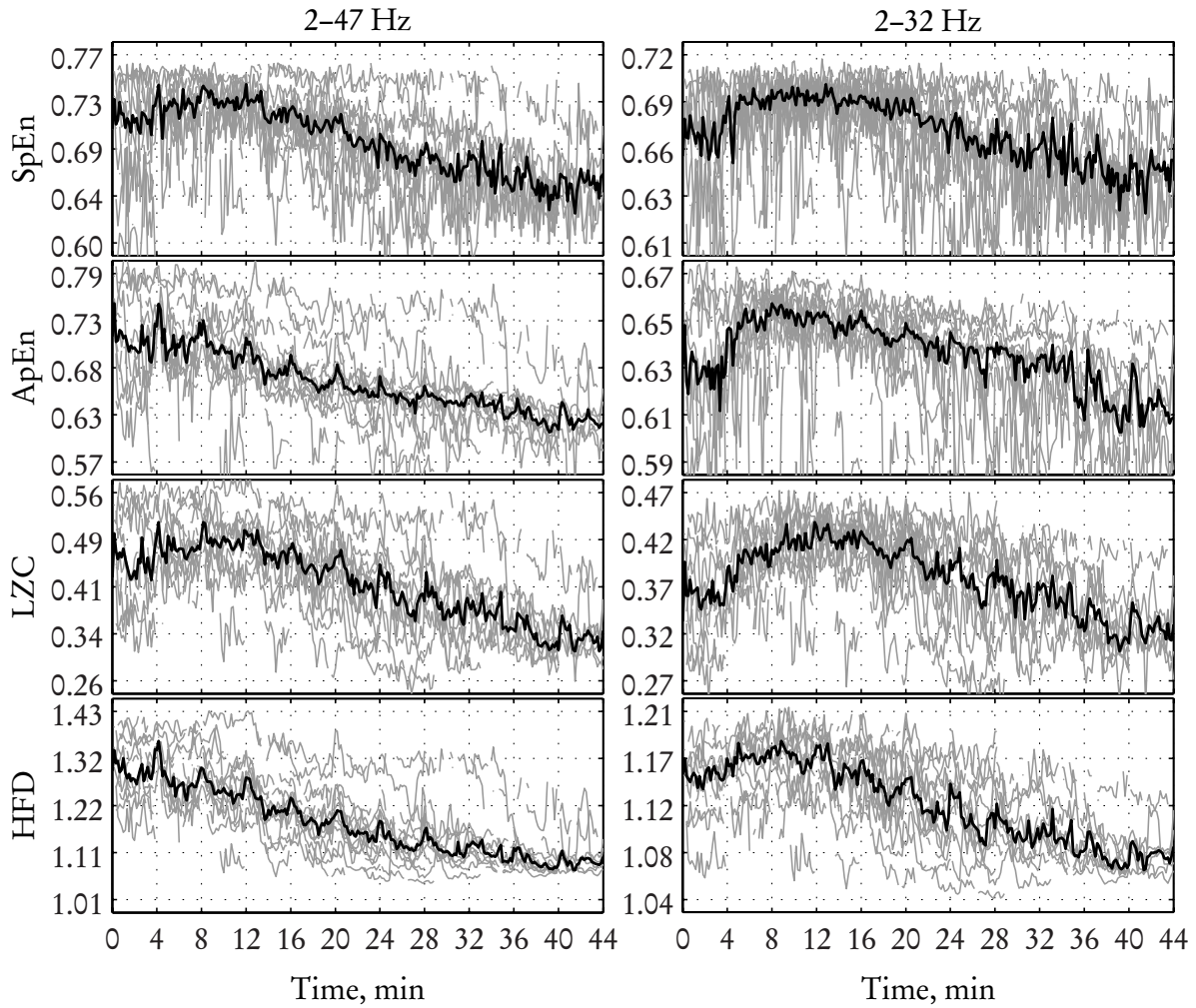

Figure 3.7 — The behavior of the regularity/complexity measures during propofol induced sedation. In the left column signals are filtered with a 2–47 Hz bandpass filter, and in the right column the bandpass filter is 2–32 Hz. The gray lines correspond to the measures calculated from the individual recordings and the thick black line is the median of the individual measures.

CHAPTER 4

Time-Frequency Analysis of the EEG Signal

Time-frequency analysis in this thesis is based on the Wigner-Ville distribution (publication **I**), Choi-Williams distribution (publication **IV**), and the generalized marginals Choi-Williams distribution with optimized kernel (publication **I**).

4.1 Overview of the Time-Frequency Analysis

The Fourier transform (FT) is a well-known method for performing spectral analysis, i.e. transforming the time-domain signal, $s(t)$, to the frequency domain, $\hat{s}(f)$. If the signal at hand consists of a transient phenomena, then the FT may not be the most suitable tool for this situation. The reason for this is the fact that the FT correlates the signal $s(t)$ with a sinusoidal wave—the domain of which covers the whole real axis. This means that $\hat{s}(f)$ depends on the values of $s(t)$ for all times t, i.e. $\hat{s}(f)$ is *global*, and therefore it is often difficult to analyze *local* properties of $s(t)$ from $\hat{s}(f)$.

To overcome this problem, in 1946 Gabor introduced the method where prior to taking the FT, the signal energy was localized by multiplying it with the translatable window function $g(t-\tau)$. By translating $g(t)$ along the signal $s(t)$ and taking the FT, one obtains a two dimensional result, called the *Gabor transform* or *short time Fourier transform*. Therefore, in the Gabor transform the signal $s(t)$ is correlated with the modulated sinusoidal waves, i.e. sinusoidals are localized in time.

Ideally, one would like to get the arbitrarily precise time and frequency information of the given signal. Unfortunately, this is not possible: the uncertainty principle states that the energy spread of the signal in time, σ_t, and in frequency, σ_f, cannot be simultaneously arbitrarily small (Cohen, 1994; Loughlin and Cohen, 2004; Mallat, 1999, chap. 4):

$$\sigma_t \sigma_f \geqslant \frac{1}{2}. \tag{4.1}$$

In Eq. (4.1) the equality holds only when the window g is a Gaussian function.

Another approach to obtain the signal energy distribution—both in time and frequency—is to correlate the signal with a time and frequency translation of itself. In this case the obtained result is a so-called quadratic time-frequency distribution (TFD). This method was first used in

quantum physics by Wigner (1932), and thereafter, it was adapted to signal processing by Ville (1948). The obtained method has a better time-frequency resolution compared to the Gabor transform. However, the most serious drawback of this kind of quadratic TFD is the existence of the so-called cross-terms (see sections 4.3 and 4.4).

The general class of quadratic TFD—the so-called Cohen's class of distributions (CCD)—was introduced by Cohen (1966, 1989). CCD covers a whole family of TFD, where for each member a different smoothing kernel for suppressing cross-terms is used. Depending on the kernel function, the distributions have different names: Choi-Williams distribution (CWD) and Born-Jordan distribution (BJD) can be mentioned as examples.

4.2 Analytic Signal

A signal $s_a(t)$ is said to be analytic if its Fourier transform is zero for negative frequencies:

$$\hat{s}_a(f) = 0 \quad \text{if} \quad f < 0. \tag{4.2}$$

A non-analytic signal $s(t)$ and its analytic version $s_a(t)$ are related through their Fourier transforms as follows (Mallat, 1999, chap. 4):

$$\hat{s}_a(f) = \begin{cases} 2\hat{s}(f) & \text{if } f \geqslant 0 \\ 0 & \text{if } f < 0. \end{cases} \tag{4.3}$$

The analytic signal $s_a(t)$ is obtained by taking the inverse Fourier transform of $\hat{s}_a(f)$ defined by the relation (4.3).

4.3 Ambiguity Function

The ambiguity function (AF) is a joint time-frequency correlation function measuring how the energy of the signal is concentrated in the time-delay versus frequency-delay plane (Hamila *et al.*, 1999; Mallat, 1999, chap. 4).

The AF of an analytic signal $s_a(t)$ is defined as follows (Mallat, 1999, chap. 4):[1]

$$\mathrm{AF}(\tau, \xi) = \int s_a\left(t + \frac{\tau}{2}\right) s_a^*\left(t - \frac{\tau}{2}\right) e^{-\jmath \xi t}\, dt, \tag{4.4}$$

where τ and ξ denote the time and frequency lag, respectively.

[1] All integrals hereafter run from $-\infty$ to $+\infty$.

If $s_a(t)$ is a composite signal consisting of two components, i.e. $s_a(t) = s_1(t) + s_2(t)$, then its AF becomes:

$$\begin{aligned}
\mathrm{AF}(\tau,\xi) &= \int \left[s_1\left(t+\frac{\tau}{2}\right) + s_2\left(t+\frac{\tau}{2}\right) \right] \left[s_1^*\left(t-\frac{\tau}{2}\right) + s_2^*\left(t-\frac{\tau}{2}\right) \right] e^{-\jmath\xi t}\, dt \\
&= \int s_1\left(t+\frac{\tau}{2}\right) s_1^*\left(t-\frac{\tau}{2}\right) e^{-\jmath\xi t}\, dt + \int s_2\left(t+\frac{\tau}{2}\right) s_2^*\left(t-\frac{\tau}{2}\right) e^{-\jmath\xi t}\, dt + \\
&\quad \int s_1\left(t+\frac{\tau}{2}\right) s_2^*\left(t-\frac{\tau}{2}\right) e^{-\jmath\xi t}\, dt + \int s_2\left(t+\frac{\tau}{2}\right) s_1^*\left(t-\frac{\tau}{2}\right) e^{-\jmath\xi t}\, dt \\
&= \mathrm{AF}_{s1}(\tau,\xi) + \mathrm{AF}_{s2}(\tau,\xi) + \text{cross-terms}
\end{aligned} \tag{4.5}$$

Eq. 4.5 shows that there are two kinds of terms in the AF of the composite signal:

1. Terms that contain only the same signal component (see the 2nd row in Eq. 4.5)—the so-called *auto-terms*.
2. Terms that contain both signal components (see the 3rd row in Eq. 4.5)—the so-called *cross-terms* (interference components). The cross-terms are generated due to the quadratic form of the AF, and their location in τ–ξ plane is determined by the time and frequency differences between signal components.

An example of a signal having two frequency components and its AF are shown in Figs. 4.1(a) and 4.1(b), respectively.

4.4 Cohen's Class of Distributions

The presence of the cross-terms in the ambiguity plane can often make the interpretation of results difficult. Therefore, one of the main problems in the time-frequency analysis is to attenuate the cross-terms and to preserve the auto-terms at the same time.

In order to attenuate the cross-terms in CCD, the AF is first multiplied by a so-called *smoothing kernel* (Cohen, 1966, 1989):

$$\mathrm{CCD}(t,f) = \iint \phi(\tau,\xi)\mathrm{AF}(\tau,\xi) e^{-\jmath\xi t} e^{-\jmath\tau f}\, d\xi\, d\tau, \tag{4.6}$$

where $\phi(\tau,\xi)$ denotes the kernel in the τ–ξ domain. Some members of the CCD are shown in Table 4.1.

It can be seen from Table 4.1 that WVD is the special case of the CCD family because there is no smoothing kernel ($\phi = 1$), and thus, the cross-terms are not attenuated at all. Therefore, if the signal at hand consists of several components, then there necessarily will be several cross-terms presented on the time-frequency plane, and the interpretation of the results can be rather complicated. On the other hand, if the given signal contains a single component, then the WVD can have resolutions superior to the other TFDs.

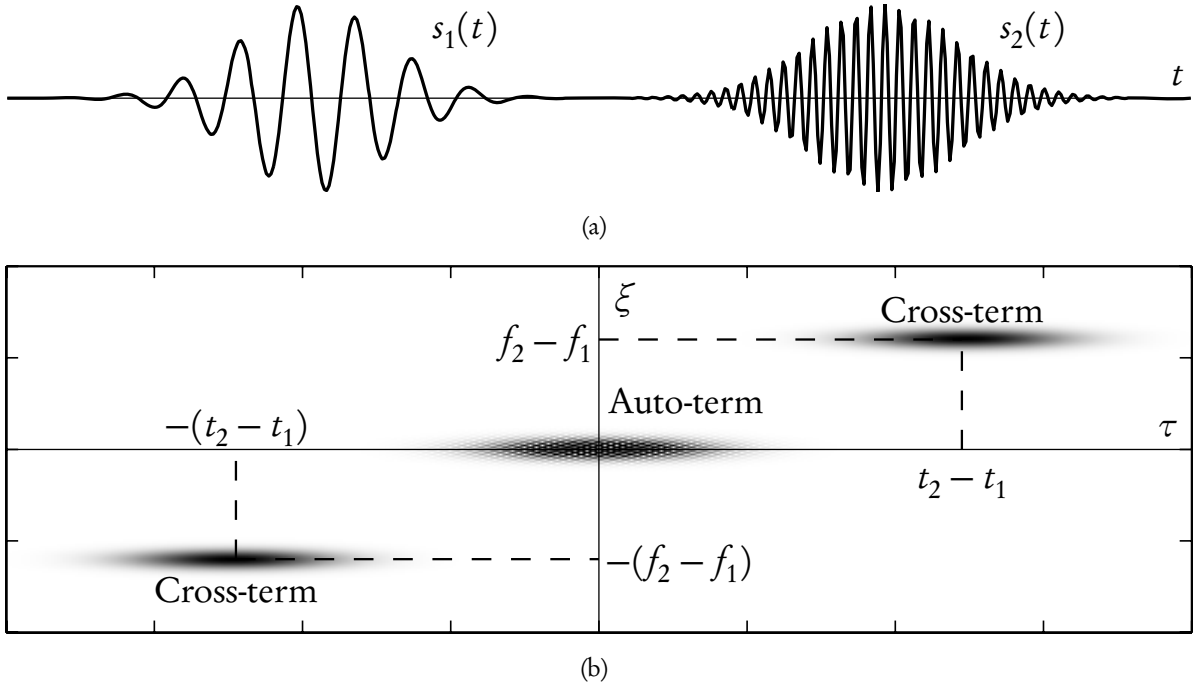

Figure 4.1 — An example of an analytic, composite signal (only the real part is shown) having two components (a) and its ambiguity function (b). t_1 and t_2 denote the occurrence in time of the first and the second component, respectively, while f_1 and f_2 denote their frequencies. Note that both auto terms are concentrated around the origin of the τ–ξ plane, while the cross-terms are located away from the origin. The location of the cross-terms are determined by the time and frequency differences between the signal components, i.e. by $t_2 - t_1$ and $f_2 - f_1$, respectively.

Table 4.1 — Examples of the TFDs belonging to the Cohen's class of distributions and their kernel functions.

TFD	**Kernel function,** $\phi(\xi, \tau)$
Wigner-Ville distribution (WVD)	1
Choi-Williams distribution (CWD)[a]	$\exp(-\tau^2\xi^2/\sigma)$
Born-Jordan distribution (BJD)	$\mathrm{sinc}(\tau\xi)$

[a] Parameter σ is used for adjusting the width of the kernel.

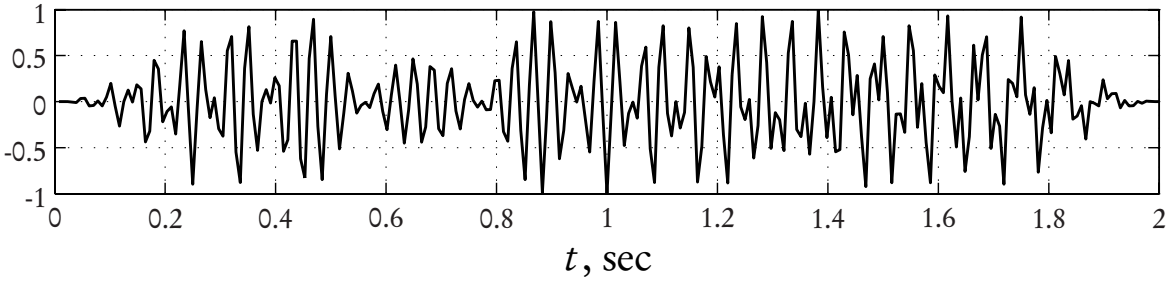

Figure 4.2 — Test signal that consists of two linear chirp components: one is increasing from 20 Hz to 50 Hz, and the other is decreasing from 40 Hz to 10 Hz.

The two remaining examples from Table 4.1, the CWD and the BJD, have smoothing kernels of exponential and sinc function shape, respectively (Williams, 1996; Choi and Williams, 1989; Cohen, 1966; Born and Jordan, 1925). While the BJD has no extra parameters, the CWD has an additional parameter, σ, for adjusting the width of the kernel. If σ is small, then the kernel quickly decreases to zero when moving away from the origin on the τ–ξ plane. This means that the cross-terms located away from the origin are attenuated effectively. The drawback here is that at the same time part of the auto-terms are suppressed as well. On the other hand, if σ has a larger value, then the shape of the kernel becomes flatter and the auto-terms are better preserved. Of course, at the same time the attenuation of the cross terms also deteriorates. At the limit $\sigma \to \infty$, the kernel function equals 1, i.e. CWD and WVD become equal:

$$\lim_{\sigma \to \infty} \mathrm{CWD} = \mathrm{WVD}. \tag{4.7}$$

An example of a signal having several components is shown in Fig. 4.2. Its AF, WVD, and CWD are presented in Figs. 4.3(a), 4.3(b), and 4.3(c), respectively.

4.5 Optimal Distributions

TFDs belonging to the Cohen's class of distributions are so-called *fixed-kernel* distributions. This means that the shape of their kernels is always the same; the shape does not depend on the signal. It is obvious that one might obtain better results if such a distribution is used, where the kernel is adapted according to the signal by some predetermined means, i.e. the distribution would have an *optimal kernel* shape according to certain criteria. Consequently, the drawback of such optimal methods is extended computational time, caused by the optimization process (Jones and Parks, 1990, 1992; Baraniuk and Jones, 1993; Jones and Baraniuk, 1995; Xia *et al.*, 1996; Davy *et al.*, 2001).

A distribution, used for an optimal approach is the generalized marginals Choi-Williams distribution (GMCWD); the kernel of which is defined as (Xia *et al.*, 1996):

$$\phi(\tau, \xi) = \exp\left[-\frac{1}{\sigma} \prod_{k=1}^{B} (\xi \cos \psi_k + \tau \sin \psi_k)^2 \right], \tag{4.8}$$

where B is the number of kernel branches, ψ_k denotes the angle of the k^{th} branch, for $k = 1,...,B$, and σ is the parameter for adjusting the widths of the branches (σ has the same role as in CWD).

Another possible kernel for optimal distribution is the so-called radially Gaussian kernel (Jones and Parks, 1990; Jones and Baraniuk, 1995):

$$\phi(\tau,\xi) = \exp\left[-\frac{\tau^2+\xi^2}{2\sigma_s^2(\psi)}\right], \tag{4.9}$$

where $\sigma_s(\psi)$ is the function that controls the spread of the kernel at the radial angle ψ. A detailed description of calculation of $\sigma_s(\psi)$ can be found in Jones and Baraniuk (1995) and Davy *et al.* (2001).

One possible way to perform an optimization is to minimize the Kullback distance d between the signal's AF given by Eq. 4.4 and the kernel given by Eq. 4.8 (Davy *et al.*, 2001):

$$d = \iint \left(\mathcal{N}\mathrm{AF}(\tau,\xi) - \mathcal{N}\phi^{\psi}(\tau,\xi)\right) \log \frac{\mathcal{N}\mathrm{AF}(\tau,\tau)}{\mathcal{N}\phi^{\psi}(\tau,\xi)} d\xi\, d\tau, \tag{4.10}$$

where ψ is the parameter being changed during optimization. $\mathcal{N}$ denotes the normalization operation applied both to the AF and the kernel function. For example, for the kernel function $\phi(\tau,\xi)$ the normalization operation $\mathcal{N}$ is defined as (Davy *et al.*, 2001)

$$\mathcal{N}\phi(\tau,\xi) = \frac{|\phi(\tau,\xi)|}{\iint |\phi(\tau,\xi)| d\xi\, d\tau}. \tag{4.11}$$

Fig. 4.3(d) illustrates the optimal GMCWD of the test signal given in Fig. 4.2. The shape of the 2-branch optimal kernel used for calculating GMCWD is shown in Fig. 4.3(e). The Kullback distance d as a function of two branch angles, ψ_1 and ψ_2, is depicted in Fig. 4.3(f). The local minimum corresponding to the optimal branch angles is marked with a circled asterisk.

4.6 Summary of the Time-Frequency Analysis

There are several different methods that allow one to obtain time-frequency representations of the signal. In general, one would like to use "the best" method, but as Cohen (1994) pointed out, there is not such a TFD that would yield the best result for all signals.

For example, if a signal at hand is a (more or less) single component signal, then WVD generally gives good results (in the way that the results are straightforwardly interpretable). On the other hand, if the signal contains several components, then the results of WVD may not be easily interpretable due to the presence of the cross-terms. In that case the use of a TFD having a smoothing kernel is obviously more justified, and probably the best results would be obtained if the optimal kernel would be used.

Fig. 4.4(a) gives an example of the EEG signal segment during propofol induced anesthesia at the burst-suppression level. The same signal as in (a) but filtered with a 3–47 Hz bandpass filter

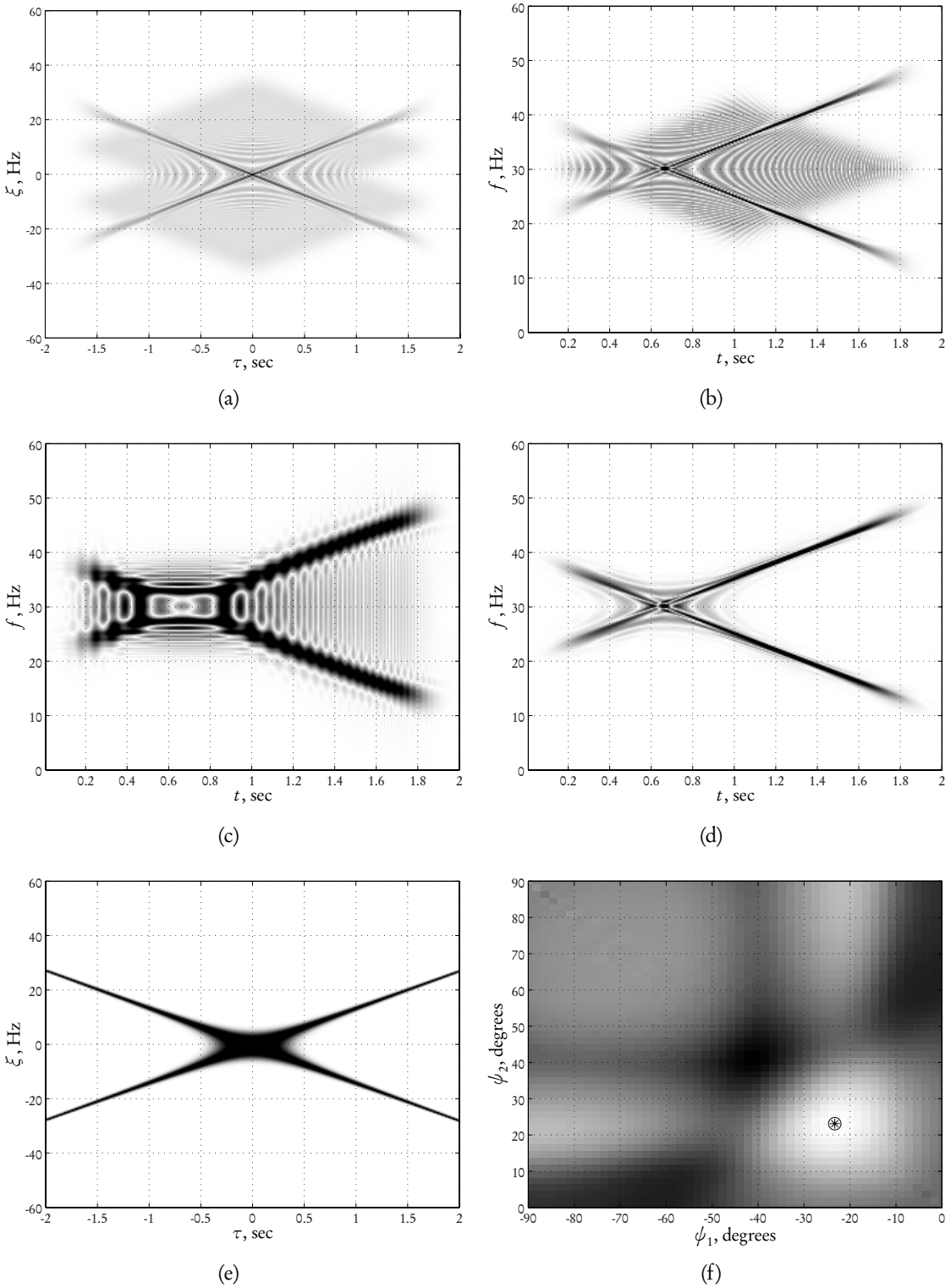

Figure 4.3 — (a): AF of the test signal given in Fig. 4.2. (b): WVD of the test signal. (c): CWD of the test signal. (d): optimal GMCWD of the test signal, $\sigma = 1$. (e): optimal 2-branch GMCWD kernel. (f): surface of the distance d as a function of two variables of ψ_1 and ψ_2 (Eq. 4.10); the location of the minimum distance is denoted by $\circledast$. All figures are gray-scale coded where white denotes the minimum value and black the maximum value, respectively.

is shown in Fig. 4.4(b). Prior to applying a time-frequency analysis, it is often useful to remove the very low-frequency components from the signal due to their (usually) large energy. The WVD of the filtered signal is illustrated in Fig. 4.4(c). By examining Fig. 4.4(c) one can identify $\approx$ 8 Hz activity appearing at around 1.5 sec and belonging to the burst. Around the same time there is additional higher-frequency activity (up to $\approx$ 25 Hz). Spindle activity at $\approx$ 14 Hz appears at around 3.5–3.6 sec. Analogously, the higher-frequency components up to $\approx$ 25 Hz are present. In addition, there appears to be $\approx 5 - 25$ Hz activity during 2.3–3.1 sec.; however, for this case it is clear that activity appearing between the burst and the spindle is actually interference caused by the cross-terms. Similarly, most of the higher-frequency components for the burst and spindle are actually cross-terms interferences, as well. Therefore, one has to be rather careful and critical while interpreting the results obtained by WVD.

Fig. 4.4(d) illustrates a time-frequency representation of the filtered EEG signal in Fig. 4.4(b) obtained by using the optimal radially gaussian kernel as described in Jones and Baraniuk (1995). It is clear that most of the interferences have been removed and thus the interpretation of the results is easier. However, when applying TFDs with an optimal kernel one has to keep in mind that these methods generally take significantly more time to compute.

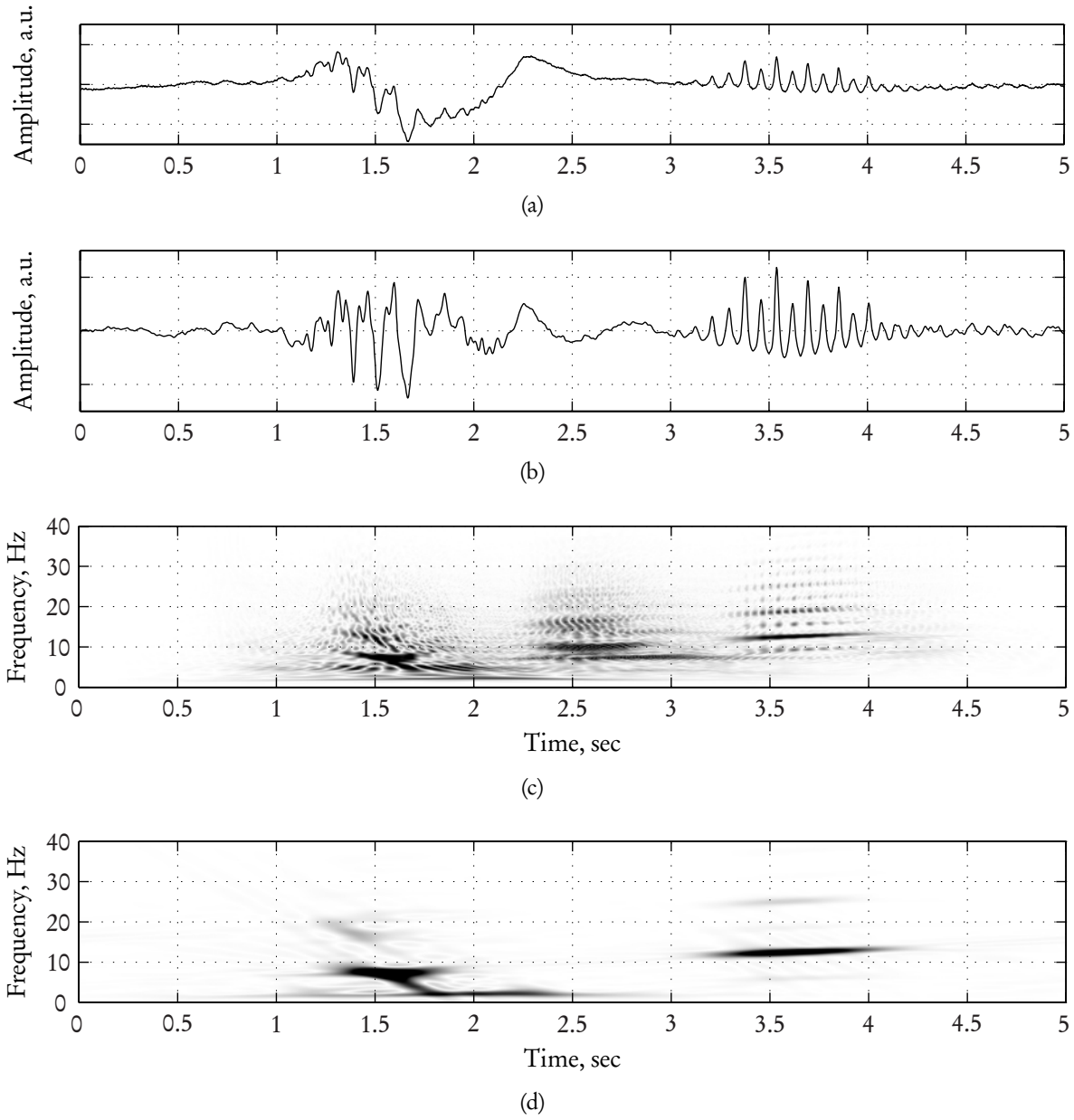

Figure 4.4 — (a): The EEG signal at the burst-suppression level during propofol anesthesia. Note that the burst pattern first appears, containing a slow-wave component with superimposed higher-frequency activity. The burst is followed by a spindle pattern. (b): The same signal as in (a) but filtered with a 3–47 Hz bandpass filter. (c): WVD of the filtered EEG signal shown in (b). (d): Time-frequency representation of the filtered EEG signal obtained using the optimal radially Gaussian kernel.

CHAPTER 5

Discussion and Concluding Remarks

The analysis of the EEG during anesthesia has been an active research field for several decades, but the real breakthrough was made about 10 years ago when the Aspect Medical Systems Inc. introduced their depth-of-anesthesia monitor based on the Bispectral Index (BIS). Since then many research groups have been working on the methods for brain monitoring during anesthesia/sedation and, as a consequence, a myriad of articles have been published.

This thesis, however, includes several new aspects, shortly listed below.

- As a part of the regularity/complexity analysis, the measure called Higuchi fractal dimension, which is relatively uncommon in EEG analysis, has been considered. One of the main advantages of this measure is the computational simplicity. The results showed that for almost all applied cases it outperformed other tested measures.

- Regularity/complexity measures have been applied to the EEG patterns occurring during burst-suppression.

- The behavior of the regularity/complexity measures has been studied using artificial surrogate signals of known properties.

- The influence of the frequency content of the EEG to the regularity/complexity measures has been studied systematically.

- The influence of remifentanil, administered together with propofol, on behavior of the regularity/complexity measures have been studied.

- Quadratic time-frequency distributions have been used to study the instantaneous frequency of the spindles during propofol induced anesthesia as well as during physiological sleep.

More detailed discussion of the above listed aspects is given in the following.

5.1 Regularity/Complexity Analysis

Regularity/complexity analysis is applied in three different cases in this thesis. Firstly, it is applied to the different EEG patterns occurring during deep propofol and sevoflurane anesthesia (burst, spindles, suppression, pre-burst-suppression EEG). Secondly, the methods are applied to the artificially generated signals—the so-called surrogate signals—having predefined power spectra as well as the probability density functions. Thirdly, they are applied to the continuous EEG signal recorded during gradually deepening sedation.

Regularity/Complexity of the EEG Burst-Suppression Patterns

In the analysis of the regularity/complexity properties of the EEG burst-suppression patterns, i.e. bursts, suppressions, and spindles, two different anesthetic drugs—propofol and sevoflurane—were considered. Additionally, in this case the EEG recordings from the conventional scalp electrodes, as well as from the depth electrodes, have been utilized. The EEG was recorded from the Parkinson disease patients who were implanted with the depth electrodes for the stimulation of the subthalamic nucleus.

The results of the analysis show that the regularity/complexity of the EEG recorded from the depth electrodes is significantly lower than that of the frontal scalp electrodes; this effect is especially clear for the sevoflurane recordings. Additionally, regularity/complexity of the EEG tends to increase from the pre-burst-suppression EEG to the bursts to the suppression. Again, this effect is more clear for the sevoflurane recordings.

The results indicate clearly that the mechanisms of propofol and sevoflurane anesthesia differ from each other and that this difference is reflected in the properties of the EEG patterns. Further interpretation of the results can be problematic since the data set was limited—in this case only four recordings were available for the analysis. Another issue is that the amplitude of the EEG during suppression periods is very low. Although the applied methods do not depend on the amplitude of the signal, the signal-to-noise ratio becomes worse as the signal amplitude decreases. Therefore, the results for the suppression periods are more reliable for the depth electrodes, since the amplitude of the signal is higher for them. In the future, this analysis should be extended to the larger number of recordings and the results should be interpreted in the light of the models describing the origin of the burst-suppression phenomenon.

Regularity/Complexity of the Surrogate Signals

It is known that the power spectrum as well as the PDF of the EEG change during anesthesia or sedation. Therefore, it would be useful to study, how different regularity/complexity measures are affected by those properties. Theoretically, Shannon entropy and spectral entropy depend only on the PDF and the power spectrum of the signal, respectively. However, in real cases, neither the PDF nor the power spectrum of the signal are generally known and, thus, they have to be estimated. Since there are several ways to estimate the PDF or the power spectrum, and these procedures always include an estimation error, the results may vary. For example, some issues related to the power spectrum estimation, in the calculation of the spectral entropy, are described by Lipping *et al.* (2005).

The study of the surrogate signals, having predefined power spectrum and PDF, shows that the remaining regularity measures used in this thesis—approximate entropy, Lempel-Ziv complexity, and Higuchi fractal dimension—are mainly dependent on the signal bandwidth; the shape of the PDF has only a minor effect. However, when the shape of the PDF is sharpening, say, when it is getting sharper than the Gaussian distribution, the dependence on the PDF increases. This effect is especially clear for the approximate entropy.

However, in this case the shapes of the power spectra of the generated surrogate signals were limited to rectangular and always centered at the half of the Nyquist frequency. One future improvement for this kind of study would be to change the shape of the surrogate signal's power spectrum to resemble more the real EEG's power spectrum.

Another interesting topic related to the surrogate analysis is the comparison of the visual appearance of surrogates having similar entropy/complexity but different shape of the power spectrum or PDF compared to a preselected EEG segment. This is especially interesting as in everyday clinical practice the EEG is interpreted mainly based on visual inspection by neurophysiologists. In section 3.1.2 of this thesis it is shown that signals of very different waveform can yield similar spectral entropy. A more systematic study including other regularity/complexity measures would be needed.

Regularity/Complexity of the EEG during Sedation

In the studies involving regularity/complexity analysis of continuous EEG the signal was recorded from the ICU patients and from the patients scheduled to undergo ambulatory surgery. For both cases the patients were sedated using propofol and, for the latter case, an opiate called remifentanil, was administered according to the previously defined protocol. Depth of sedation was assessed clinically using the Ramsay score or the modified OAA/S score.

In this case the regularity/complexity measures were calculated in a moving analysis window and their correlation with the Ramsay score and the modified OAA/S was studied. Additionally, the influence of remifentanil to the behavior of the regularity/complexity measures was estimated.

An important aspect one has to keep in mind when performing the regularity/complexity analysis, is the EEG frequency band used for the analysis. It means that one has to carefully select the cutoff frequencies for the low-pass and high-pass filters. In this thesis the following three lower cutoff frequencies for the EEG frequency band have been used: 0.5 Hz, 2 Hz, and 6 Hz. The higher cutoff frequencies were selected as 19 Hz, 32 Hz, and 47 Hz. This particular selection of the lower cutoff frequencies was made to cover the rather wide range of lower cutoff frequencies used in commercial depth-of-anesthesia monitors. For example, the SNAP® monitor by Viasys Healthcare (USA) has lower cutoff frequency 0.1 Hz while that of the CSI® monitor by Danmeter A/S (Denmark) is as high as 6 Hz.

Selecting the higher cutoff frequency for the EEG frequency band involves a trade-off, especially if the EEG during sedation is considered. Namely, it is known that the frequency band of the EEG during sedation can extend up to 40 Hz or even higher. However, the high-frequency component of the EEG can be contaminated by the muscle activity, especially when the patient is waking up from sedation. Although the muscle activity is noise from the EEG point of

view, it can be utilized for the early detection of arousal from sedation. Rautee *et al.* (2004) have found that for the depth-of-sedation analysis 20 Hz is the effective border-frequency between the EEG and the muscle activity. However, from neurophysiology it is known that muscle activity can cause frequency components of as low frequency as 5 Hz or even lower. Therefore, to minimize the effect of muscle activity in the analysis, 19 Hz was selected as the lowest value for the higher cutoff frequency. The higher upper edges of the EEG frequency band—32 Hz and 47 Hz—are inspired by the commercial Entropy® monitor by GE Healthcare.

Usually it is assumed that the EEG signal becomes more regular—entropy decreases—as anesthesia/sedation is deepening. However, since different methods take into account different properties of the signal, the results can be contradictory. For example, the Shannon entropy increases with deepening sedation, as pointed out by Bruhn *et al.* (2001b) as well as in the publication **III**.

The results clearly show that despite the fact that the applied regularity measures (except spectral entropy) do not directly depend on the power spectrum, they are still very sensitive to the frequency content of the signal. This, in turn, can cause the situation where the monotonically decreasing behavior of the presented regularity measures is lost when high frequencies are cut off and/or low frequencies are preserved. In this situation typically the so-called biphasic behavior—at the lighter levels of sedation EEG regularity/complexity increases with deepening sedation, while at deeper levels the change is the opposite—occurs. The length and the steepness (for the increasing and decreasing phase) of the different phases depends on the exact selection of the cutoff frequencies.

5.2 Time-Frequency Analysis

In this thesis the time-frequency analysis is concentrated on the EEG spindle patterns. The main idea behind the analysis is to investigate the instantaneous frequency of the spindles during propofol anesthesia and, in addition, to perform the comparison with spindles occurring during physiological sleep.

Propofol spindles can contain two (or even more) waxing and waning oscillations, which are easily distinguishable by visual observation. An example of such waveform is given in Fig. 5.1(a). Another property of propofol spindle waveforms is the appearance of higher frequency components—they appear at twice, sometimes even at triple, of the principal frequency of the spindle (see time-frequency representations in Fig. 5.1). Additionally, in propofol anesthesia part of the spindle sometimes transforms to another rhythm of the main harmonic frequency, and the so-called "breaking" waveform appears. Such case is illustrated in Fig. 5.1(b). However, it remains to be investigated whether or not these two harmonic-producing phenomena have the same origin.

The analysis of instantaneous frequency of the spindles has revealed that the angle of its trend is generally very small, meaning that the principal frequency of a given spindle is relatively stable. However, occasionally spindles can show either increasing or decreasing trend in the instantaneous frequency. For example, the spindle presented in Fig. 5.1(a) demonstrates slightly increasing instantaneous frequency.

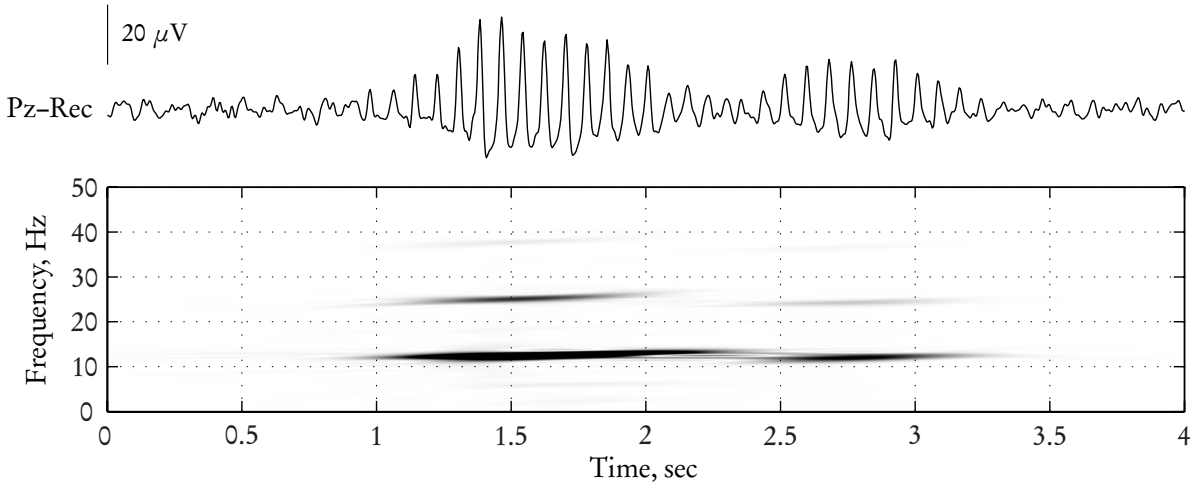

(a) A spindle having two oscillating components

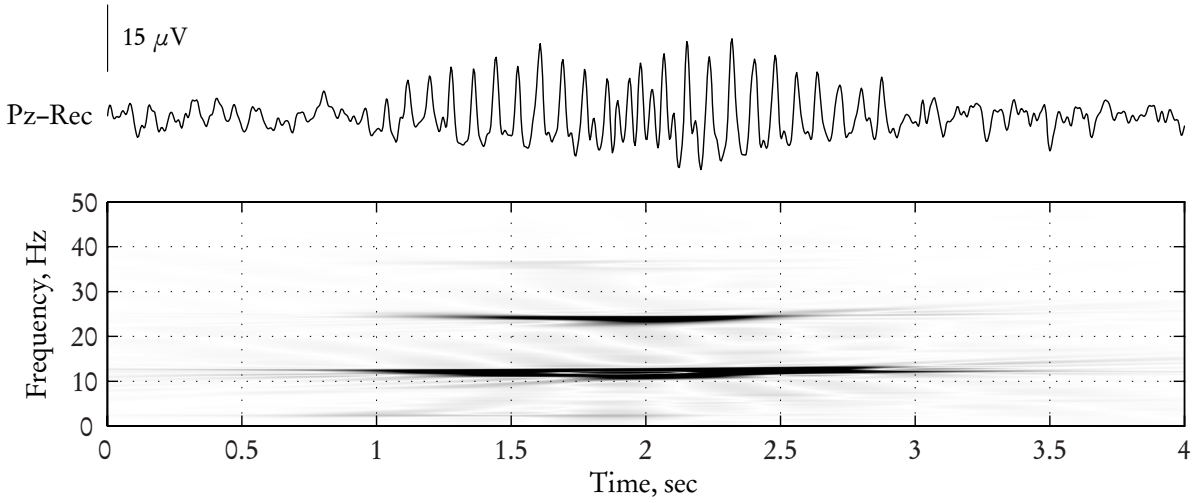

(b) A spindle having "breaking" waveform

Figure 5.1 — Examples of the spindle structures during propofol induced anesthesia. (a): A spindle having two waxing-waning oscillations and its time-frequency representation; (b): a spindle having the so-called "breaking" waveform in its time-frequency representation. Time-frequency representations for both cases are calculated using the optimally radial Gaussian kernel. The time axis is the same for the given spindle waveform and the corresponding time-frequency representation

Comparison between the spindles during propofol induced anesthesia and physiological sleep shows that the average frequency of the propofol spindles is slightly higher than that of the sleep spindles. But, nevertheless, it still fits into the frequency range considered typical to sleep spindles in general.

CHAPTER **6**

Summary of the Publications and the Author's Contribution

This thesis includes five original publications, which can be divided into two subcategories: regularity and time-frequency analysis of the EEG signal. Publications **II**, **III**, and **V** deal with the regularity analysis, whereas, publication **I** concentrates on the time-frequency analysis. Exceptionally, publication **IV** deals with both regularity and time-frequency analysis. Subsequently, a short summary of each publication as well as the author's contribution to each paper is given.

Publication **I** concentrates on two time-frequency methods—WVD and GMCWD with an optimized kernel—which have been applied to the spindle patterns occurring during propofol induced anesthesia. The results from this study show that the instantaneous frequency of the spindle during deep propofol anesthesia show a slightly decreasing trend. The comparison between the two methods yields that by using GMCWD with an optimized kernel, it is possible to obtain slightly better results by means of mean square error. However, the cost of this was a significantly larger computational load. The author performed all analyses and is the first author of the article.

Publication **II** compares the regularity/complexity measures—SpEn, ApEn, LZC, and HFD—applied to the different signal patterns recorded during propofol as well as sevoflurane anesthesia. The signal patterns included bursts and suppression periods (for both propofol and sevoflurane) as well as spindles (only for propofol). In addition, this study makes a comparative analysis between signals recorded by using conventional surface electrodes and depth electrodes. The results show that the complexity of the EEG increases from the pre-burst-suppression pattern, to the bursts and to the suppression. This tendency is more emphasized in sevoflurane recordings. The author performed all analyses included in this study and is the first author. This work participated in the student paper competition of the 5th International Workshop on Biosignal Interpretation (Tokyo, Japan, Sept. 6–8 2005) where it won second place.

Publication **III** can be divided into two parts, where ShEn in addition to the regularity measures listed for publication **II** are applied 1) to the artificially generated surrogate signals, and 2) to the EEG signals. The artificial signals were generated so that both their PDFs and power spectra were previously fixed. The idea of such an analysis was to determine how the regularity measures listed above are influenced by the shape of the PDF and power spectrum of the signal. The result of the first part shows that ShEn and SpEn expectedly depend only on one property, i.e. on the PDF or the power spectrum, respectively, while ApEn, LZC, and HFD depend on both properties. Secondly, the measures were applied to the EEG signals recorded in the ICU during propofol induced sedation. Prior to applying the regularity measures, the EEG

signal was low-pass filtered by using several cut-off frequencies. In addition, we used an analysis window of several lengths. The results show that ApEn, LZC, and HFD are more strongly dependent on the presence of high frequencies than other measures. Additionally, SpEn, calculated using the fast Fourier transform for power spectrum estimation, is more sensitive to the length of the analysis window. The comparison with the Ramsay scores (clinical assessment of depth of sedation) reveals that while ShEn remains constant or slightly increases with deepening sedation, the other measures tend to decrease. The author performed all analyses related to the artificial signals and is the the first author.

Publication **IV** compares the properties of the EEG spindle patterns corresponding to two different phenomena: natural sleep and propofol anesthesia. In this study, the time-frequency method CWD was applied in order to obtain the intraspindle mean frequency and the angle of the trend at an instantaneous frequency. In addition, three regularity measures—SpEn, ApEn, and HFD—were applied. The statistical analysis revealed that all measures, except ApEn, were able to separate these two types of EEG spindles. The author performed all analyses included in this study and is the first author.

Publication **V** gives an overview of the study, where 45 patients were randomly divided into three groups according to the dose of remifentanil (0, 2, or 4 ng/ml) administered. Additionally, all patients received a stepwise-increased, effect-site concentration controlled dose of propofol. At every step of propofol concentration increase, the OAA/S score was assessed. The EEG signal was segmented into 15 sec segments, and for each segment, the SpEn, ApEn, LZC, HFD, relative beta ratio, and SyncFastSlow measure were calculated. In addition, the state entropy and response entropy from the AS/5 Anesthesia monitor were included in the comparison. The goal of this study was to analyze the influence of remifentanil as well as the frequency content of the EEG to the performance of the above listed measures. The results show that regularity measures are highly sensitive to the frequency content of the signal as well as to the dose of remifentanil. By means of the prediction probability, the most discriminative measure with respect to OAA/S score was HFD, which even outperformed response entropy and state entropy. The author performed all analyses included in this study and was the first author.

In all the above listed publications, especially the supervisor of the thesis, Prof. Tarmo Lipping, as well as M.D, Ph.D Ville Jäntti, M.D Pasi Puumala, and Prof. Michel Struys, gave valuable comments and were also co-writers of the publications.

Appendices

APPENDIX **A**

A Brief History of Entropy

Despite the fact that the concept of entropy has been widely used in the field of signal processing for characterizing regularity properties of the signal, its origin is in physics, more precisely in thermodynamics (Darrow, 1944; Machta, 1999; Ambegaokar and Clerk, 1999). In statistical thermodynamics the word *entropy* has been used to characterize a system's "disorder", "randomness", "dispersion", "homogeneity", or even "mixed-up-ness" (Styer, 2000).

Entropy as in Classical Thermodynamics

In 1854 Rudolf Clausius, a German physicist and mathematician, published a paper where for the first time the mathematical formulation of entropy was given. Clausius was further developing the ideas of Sadi Carnot, a French physicist and engineer, who in the beginning of the 19th century worked on heat engines (he invented an ideal heat engine, the so-called Carnot cycle) and formulated the first steps towards the second law of thermodynamics. In this paper Clausius stated that in any real process a small amount of heat energy dQ is wasted across the system boundary, i.e. there always will be energy loss. Clausius gave the energy loss the following formulation:

$$dS = \frac{dQ}{T}, \tag{A.1}$$

where T is the absolute temperature, dQ is the amount of heat added or removed from the system, and dS is the change of entropy. However, the quantity S got the name *entropy* only in 1865 when Clausius published another paper on thermodynamics (Cropper, 2001). According to Laidler (1995), Clausius wrote:

> *I propose to name the quantity S the entropy of the system, after the Greek word [trope], the transformation. I have deliberately chosen the word entropy to be as similar as possible to the word energy: the two quantities to be named by these words are so closely related in physical significance that a certain similarity in their names appears to be appropriate.*

As formulated by Clausius, the concept of entropy in classical thermodynamics literally means the transformation of energy. Entropy here can be thought of as the *macroscopic* scale (large-scale) measure.

Entropy as in Statistical Thermodynamics

In 1877 Ludwig Boltzmann, an Austrian physicist, introduced an alternative formulation of entropy, the *microscopic* entropy:

$$S = k_B \log \Omega, \tag{A.2}$$

where k_B is Boltzmann's constant and Ω is the number of microstates within the given macrostate. Boltzmann's entropy formula can be manipulated into the formula (Machta, 1999; Styer, 2000):

$$S = -k_B \sum_i p_i \log p_i, \tag{A.3}$$

where the sum goes over the microstates i of the system and p_i is the probability that i^{th} microstate of the given macrostate is occupied.

Entropy described by (A.2) or (A.3) is usually thought of as a measure of statistical disorder of the system.

A generalized form of Boltzmann entropy, i.e. (A.3), is the so-called *Tsallis entropy* (Tsallis, 2002):

$$S_q = \frac{k_B}{q-1}\left(1 - \sum_i p_i^q\right), \tag{A.4}$$

where q is a real parameter. In the limit $q \to 1$ Boltzmann entropy is obtained.

Entropy as in Information Theory

In 1948 Claude Shannon, an American engineer and mathematician, published the work where the theoretical basis for the transmission of signals between a transmitter and receiver was founded. He derived an expression for describing information flow H, which he was going to call the "measure of uncertainty". However, the story goes that Shannon was convinced to use the name of "entropy" instead of "uncertainty", and according to Tribus and McIrvine (1971), Shannon said:

> *My greatest concern was what to call it. I thought of calling it "information", but the word was overly used, so I decided to call it "uncertainty". When I discussed it with John von Neumann, he had a better idea. Von Neumann told me, "You should call it entropy, for two reasons. In the first place your uncertainty function has been used in statistical mechanics under that name, so it already has a name. In the second place, and more important, nobody knows what entropy really is, so in a debate you will always have the advantage".*

Shannon entropy, defined as

$$H_{Sh} = -\sum_i p_i \log p_i, \tag{A.5}$$

has almost the same formulation as Boltzmann entropy (A.3); the important difference is the absence of Boltzmann's constant. Therefore, Shannon entropy has no physical units.

A generalization of Shannon entropy is the so-called *Rényi entropy*, introduced by Alfred Rényi (1995), which defines a family of entropies used for quantifying the randomness of the system (Kantz and Schreiber, 1997). The Rényi entropy of order q, where $q > 0$, is defined as:

$$H_q = \frac{1}{1-q} \log \sum_i p_i^q \tag{A.6}$$

In the limit $q \to 1$ Rényi entropy H_1 converges to Shannon entropy (A.5).

APPENDIX **B**

Phase-Space Concept and Correlation Dimension

Phase-Space Concept

Dynamical systems are often described by using the *phase-space* (also known as a *state-space*) concept. In this approach it is assumed that the state of a system can be described by a set of d state variables so that each state of the system corresponds to a point $\zeta \in \mathbb{R}^d$, where $\mathbb{R}^d$ is a d-dimensional Euclidean space. $\mathbb{R}^d$ is called the *true phase-space* and d the *true phase-space dimension*.

Since the state of a dynamical system is changing with time, the state $\zeta(t)$ is a function of time. If the current state $\zeta(0)$ uniquely determines the future states, i.e. $\zeta(t)$, $t > 0$, the system is a *deterministic dynamical system*.

Usually, however, it is not possible to observe directly the true states $\zeta(t)$ of a dynamical system. Typically, one has obtained only the time series of measurements $x(t) = h(\zeta(t))$ by applying some measurement function h to the true states ζ. Thus, the measurement function h usually transforms the true states ζ to the lower dimensional space ($\mathbb{R}^d \to \mathbb{R}^{d'}$, $d' < d$), where frequently $d' = 1$, i.e. the obtained time series is one dimensional.

A continuous time deterministic dynamical system can be described by a set of differential equations

$$\dot{\zeta} = \mathbf{F}(\zeta(t)), \tag{B.1}$$

where $\mathbf{F}$ is a smooth vector field in $\mathbb{R}^d$. Depending on the structure of $\mathbf{F}$, there are several possibilities for the behavior of $\zeta(t)$ as $t \to \infty$. If the dynamical system is dissipative and bounded, then after a sufficiently long, time the system will be attracted to some sub-set of phase-space, which is called an *attractor*. There are four types of attractors: fixed points, limit cycles, limit tori, and strange attractors. It is characteristic for chaotic systems that their attractors are geometrically complicated objects, typically having fractal, i.e. self-similar, structure; therefore, such attractors are called *strange attractors*.

One of the most frequently used examples for illustrating deterministic chaotic systems is the so-called *Lorenz system*, which is given by the following differential equations (Lorenz, 1963):

$$\begin{cases} \dot{x}(t) = \sigma\,(y(t) - x(t)) \\ \dot{y}(t) = r\,x(t) - y(t) - x(t)z(t) \\ \dot{z}(t) = x(t)y(t) - b\,z(t). \end{cases} \tag{B.2}$$

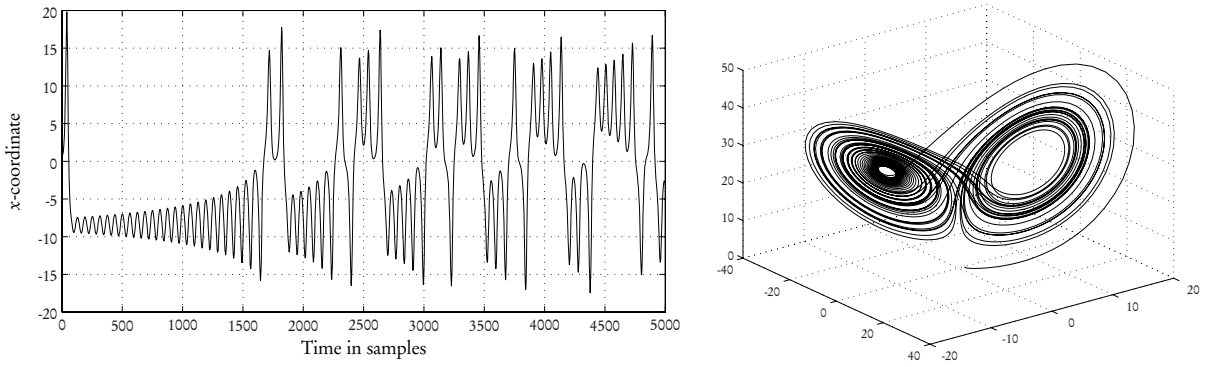

Figure B.1 — (a): Numerically integrated x-coordinate of the Lorenz system. (b): Phase-space representation of the Lorenz system. The parameters are chosen as $\sigma = 10$, $r = 28$, and $b = 8/3$ for both cases.

The parameters are traditionally chosen as $\sigma = 10$, $r = 28$, and $b = 8/3$. The x-coordinate and attractor in phase-space of the Lorenz system is shown in Fig. B.1.

Before applying further analysis, the phase-space has to be reconstructed from the measurement signal $x(t)$. Thus, the measurements have to be transformed somehow into the *reconstructed vectors* $\mathbf{x} \in \mathbb{R}^m$, where m is the *embedding dimension*. One possibility to obtain the reconstructed vectors is to use *time-delayed embedding*:

$$\mathbf{x}(t) = \big(x(t), x(t-\tau), x(t-2\tau), \ldots, x(t-(m-1)\tau)\big), \tag{B.3}$$

where τ is the difference in samples between adjacent components of the delay vectors. τ is also called the *delay time*.

Another problem one has to deal with before applying delay reconstruction is that neither the embedding dimension m nor time delay τ is generally known a priori. A comprehensive overview about finding good embedding parameters, i.e. m and τ, is given by Kantz and Schreiber (1997) and Galka (2000).

Correlation Dimension

One possibility to quantify self-similarity or fractality of a geometrical object reconstructed from a finite set of data points is the so-called *correlation dimension D*, introduced by Grassberger and Procaccia (1983). In order to obtain the correlation dimension first the so-called correlation sum for a collection of reconstructed phase-space points $\mathbf{x}$ is formed. The classical formula for the correlation sum is the following:

$$C(r) = \frac{2}{N(N-1)} \sum_i \sum_{j>i} \Theta(r - \|\mathbf{x}_i - \mathbf{x}_j\|), \tag{B.4}$$

where r is a predefined distance in phase-space, and Θ is the Heaviside function defined as

$$\Theta(x) = \begin{cases} 0 & \text{if } x \leqslant 0 \\ 1 & \text{if } x > 0. \end{cases} \tag{B.5}$$

Thus, the correlation sum defined by Eq. B.4 counts pairs $(\mathbf{x}_i, \mathbf{x}_j)$ whose distance is smaller than r. If the amount of data is growing to infinity ($N \to \infty$) and distance r is converging to zero ($r \to 0$), then C is expected to scale according to the power law, $C(r) \propto r^D$, where D is the correlation dimension. Thereafter, the correlation dimension D is defined as

$$D = \lim_{r \to 0} \lim_{N \to \infty} \frac{\partial \log C(r)}{\partial \log r} \tag{B.6}$$

The calculation of a correlation dimension from the time series, as well as accompanying pitfalls and interpretation problems, are described in a very detailed manner by Kantz and Schreiber (1997).

Bibliography

D. Abásolo, R. Hornero, P. Espino, D. Álvarez, and J. Poza (2006a). "Entropy analysis of the EEG background activity in Alzheimer's disease patients." *Physiological Measurement*, **27**(3):241–253.

D. Abásolo, R. Hornero, P. Espino, J. Poza, C. I. Sánchez, and R. de la Rosa (2005). "Analysis of regularity in the EEG background activity of Alzheimer's disease patients with approximate entropy." *Clinical Neurophysiology*, **116**(8):1826–1834.

D. Abásolo, R. Hornero, C. Gómez, M. García, and M. López (2006b). "Analysis of EEG background activity in Alzheimer's disease patients with Lempel-Ziv complexity and central tendency measure." *Medical Engineering and Physics*, **28**:315–322.

A. Accardo, M. Affinito, M. Carrozzi, and F. Bouquet (1997). "Use of the fractal dimension for the analysis of electroenchepalographic time series." *Biological Cybernetics*, **77**:339–350.

L. Aftanas and S. Golosheykin (2005). "Impact of regular meditation practice on EEG activity at rest and during evoked negative emotions." *International Journal of Neuroscience*, **115**(6):893–909.

V. Ambegaokar and A. A. Clerk (1999). "Entropy and time." *American Journal of Physics*, **67**:1068–1073.

American Electroencephalographic Society (1994). "Guideline thirteen: guidelines for standard electrode position nomenclature." *Journal of Clinical Neurophysiology*, **11**:111–113.

F. Amzica and M. Steriade (1995). "Short- and long-range neuronal synchronization of the slow (< 1 hz) cortical oscillation." *Journal of Neurophysiology*, **73**(1):20–38.

R. E. Anderson and J. G. Jakobsson (2004). "Entropy of EEG during anaesthetic induction: a comparative study with propofol or nitrous oxide as sole agent." *British Journal of Anesthesiology*, **92**(2):167–170.

A. Anier, T. Lipping, S. Melto, and S. Hovilehto (2004). "Higuchi fractal dimension and spectral entropy as measures of depth of sedation in intensive care unit." In "Proceedings of the 26th Annual International Conference of IEEE EMBS," pages 526–529. San Francisco, USA.

J. E. Arle and R. H. Simon (1990). "An application of fractal dimension to the detection of transients in the electroencephalogram." *Electroencephalography and Clinical Neurophysiology*, **75**(4):296–305.

R. G. Baraniuk and D. L. Jones (1993). "A signal-dependent time-frequency representation: optimal kernel design." *IEEE Transactions on Signal Processing*, **41**:1589–1602.

G. Barr, J. G. Jakobsson, A. Owall, and R. E. Anderson (1999). "Nitrous oxide does not alter bispectral index: study with nitrous oxide as sole agent and as an adjunct to i.v. anaesthesia."

British Journal of Anaesthesia, **82**(6):827–830.

A. Bashashati, R. K. Ward, G. E. Birch, M. R. Hashemi, and M. A. Khalilzadeh (2003). "Fractal dimension-based EEG biofeedback system." In "Proceedings of the 25th Annual International Conference of IEEE EMBS," pages 2220–2223. Cancun, Mexico.

M. Bazhenov, I. Timofeev, M. Steriade, and T. Sejnowski (2000). "Spiking-bursting activity in the thalamic reticular nucleus initiates sequences of spindle oscillations in thalamic networks." *Journal of Neurophysiology*, **84**(2):1076–1087.

J. Bercher and C. Vignat (2000). "Estimating the entropy of a signal with applications." *IEEE Transactions on Signal Processing*, **48**:1687–1694.

H. Berger (1929). "Über das Elektroenkephalogramm des Menschen (About the human electroencephalogram. In German)." *Archiv für Psychiatrie und Nervenkrankheiten*, **87**:527–570.

A. Bezerianos, S. Tong, and N. Thakor (2003). "Time-dependent entropy estimation of EEG rhythm changes following brain ischemia." *Annals of Biomedical Engineering*, **31**:221–232.

M. Born and P. Jordan (1925). "Zur Quantenmechanik." *Zeitschrift für Physik*, **34**:858–888.

T. W. Bouillon, J. Bruhn, L. Radulescu, C. Andresen, T. J. Shafer, C. Cohane, and S. L. Shafer (2004). "Pharmacodynamical interaction between propofol and remifentanil regarding hypnosis, tolerance of laryngoscopy, bispectral index, and electroencephalograpic approximate entropy." *Anesthesiology*, **100**:1353–1372.

J. Bruhn, T. W. Bouillon, A. Hoeft, and S. L. Shafer (2002). "Artifact robustness, inter- and intraindividual baseline stability, and rational EEG parameter selection." *Anesthesiology*, **96**:54–59.

J. Bruhn, T. W. Bouillon, L. Radulescu, A. Hoeft, E. Bertaccini, and S. L. Shafer (2003). "Correlation of approximate entropy, bispectral index, and spectral edge frequency 95 (SEF95) with clinical signs of "anesthetic depth" during coadministration of propofol and remifentanil." *Anesthesiology*, **98**(3):621–627.

J. Bruhn, T. W. Bouillon, and S. L. Shafer (2000a). "Electromyographic activity falsely elevates the Bispectral index." *Anesthesiology*, **92**(5):1485–1487.

J. Bruhn, T. W. Bouillon, and S. L. Shafer (2001a). "Onset of propofol-induced burst suppression may be correctly detected as deepening of anaesthesia by approximate entropy but not by bispectral index." *British Journal of Anesthesiology*, **87**(3):505–507.

J. Bruhn, L. E. Lehmann, H. Röpcke, T. W. Bouillon, and A. Hoeft (2001b). "Shannon entropy applied to the measurement of the electroencephalographic effects of desflurane." *Anesthesiology*, **95**:30–35.

J. Bruhn, H. Röpcke, and A. Hoeft (2000b). "Approximate entropy as an electroencephalographic measure of anestetic drug effect during desflurane anesthesia." *Anesthesiology*, **92**:715–726.

J. Bruhn, H. Röpcke, B. Rehberg, T. Bouillon, and A. Hoeft (2000c). "Electroencephalogram approximate entropy correctly classifies the occurence of burst suppression pattern as increasing anesthetic drug effect." *Anesthesiology*, **93**:981–985.

N. Burioka, G. Cornélissen, F. Halberg, D. T. Kaplan, H. Suyama, T. Sako, and E. Shimizu (2003). "Approximate entropy of human respiratory movement during eye-closed waking and different sleep stages." *Chest*, **123**:80–86.

N. Burioka, G. Cornélissen, Y. Maegaki, F. Halberg, D. T. Kaplan, M. Miyata, Y. Fukuoka, M. Endo, H. Suyama, Y. Tomita, and E. Shimizu (2005a). "Approximate entropy of the electroencephalogram in healthy awake subjects and absence epilepsy patients." *Clinical EEG and Neuroscience*, **36**(3):188–193.

N. Burioka, M. Miyata, G. Cornélissen, F. Halberg, T. Takeshima, D. T. Kaplan, H. Suyama, M. Endo, Y. Maegaki, T. Nomura, Y. Tomita, K. Nakashima, and E. Shimizu (2005b). "Approximate entropy in the electroencephalogram during wake and sleep." *Clinical EEG and Neuroscience*, **36**:21–24.

N. Burioka, H. Suyama, T. Sako, M. Miyata, T. Takeshima, M. Endo, J. Kurai, Y. Fukuoka, M. Takata, T. Nomura, K. Nakashima, and E. Shimizu (2002). "Non-linear dynamics applied to human respiratory movement during sleep." *Biomedicine and Pharmacotherapy*, **56 Suppl 2**:370–373.

W. B. Cammarano, J. F. Pittet, S. Weitz, R. M. Schlobohm, and J. D. Marks (1998). "Acute withdrawal syndrome related to the administration of analgesic and sedative medications in adult intensive care unit patients." *Critical Care Medicine*, **26**(4):676–684.

D. A. Chernik, D. Gillings, H. Laine, J. Hendler, J. M. Silver, A. B. Davidson, E. M. Schwam, and J. L. Siegel (1990). "Validity and reliability of the Observer's Assessment of Alertness/Sedation scale: study with intravenous midazolam." *Journal of Clinical Psychopharmacology*, **10**(4):244–251.

H.-I. Choi and W. J. Williams (1989). "Improved time-frequency representation of multicomponent signals using exponential kernels." *IEEE Transactions on Acoustics, Speech and Signal Processing*, **37**(6):862–871.

L. Cohen (1966). "Generalized phase-space distribution functions." *Journal of Mathematical Physics*, **7**:781–786.

L. Cohen (1989). "Time-frequency distributions—a review." *Proceedings of the IEEE*, **77**(7):941–981.

L. Cohen (1994). "The uncertainty principle in signal analysis." In "Proceedings of the IEEE-SP International Symposium on Time-Frequency and Time-Scale Analysis," pages 182–185.

W. H. Cropper (2001). *Great physicists: The life and times of leading physicists from Galileo to Hawking.* Oxford University Press.

K. K. Darrow (1944). "The concept of entropy." *American Journal of Physics*, **12**:183–196.

A. J. Davidson and C. Czarnecki (2004). "The Bispectral Index in children: comparing isoflurane and halothane." *British Journal of Anaesthesia*, **92**(1):14–17.

M. Davy, C. Doncarli, and G. F. Bordeaux-Bartels (2001). "Improved optimization of time-frequency-based signal classifiers." *IEEE Signal Processing Letters*, **8**:52–57.

P. J. Durka, U. Malinowska, W. Szelenberger, A. Wakarow, and K. J. Blinowska (2005). "High resolution parametric description of slow wave sleep." *Journal of Neuroscience Methods*, **147**:15–21.

J.-P. Eckmann and D. Ruelle (1985). "Ergodic theory of chaos and strange attractors." *Reviews of Modern Physics*, **88**:617–656.

A. Ekman, M.-L. Lindholm, C. Lennmarken, and R. Sandin (2004). "Reduction in the incidence of awareness using BIS monitoring." *Acta Anaesthesiologica Scandinavica*, **48**(1):20–26.

R. K. Ellerkmann, V.-M. Liermann, T. M. Alves, I. Wenningmann, S. Kreuer, W. Wilhelm, H. Roepcke, A. Hoeft, and J. Bruhn (2004). "Spectral entropy and bispectral index as measures of the electroencephalographic effects of sevoflurane." *Anesthesiology*, **101**:1275–1282.

R. Esteller, G. Vachtsevanos, J. Echauz, and B. Lilt (1999). "A comparison of fractal dimension algorithms using synthetic and experimental data." In "Proceedings of the 1999 IEEE International Symposium on Circuits and Systems," volume 3, pages 199–202.

R. Esteller, G. Vachtsevanos, J. Echauz, and B. Lilt (2001). "A comparison of waveform fractal dimension algorithms." *IEEE Transactions on Circuits and Systems—I: Fundamental Theory and Applications*, **48**:177–183.

J. Fell, G. Fernández, and C. E. Elger (2003). "More than synchrony: EEG chaoticity may be necessary for conscious brain functioning." *Medical Hypotheses*, **61**:158–160.

M. Ferrario, M. G. Signorini, G. Magenes, and S. Cerutti (2006). "Comparison of entropy-based regularity estimators: application to the fetal heart rate signal for the identification of fetal distress." *IEEE Transactions on Biomedical Engineering*, **53**:119–125.

D. Gabor (1946). "Theory of communication." *Journal of IEE*, **93**:429–457.

A. Galka (2000). *Topics in nonlinear time series analysis: with implications for EEG analysis.*, volume 14 of *Advanced series of nonlinear dynamics*. World Scientific Publishing Co., Singapore.

P. S. Glass, M. Bloom, L. Kearse, C. Rosow, P. Sebel, and P. Manberg (1997). "Bispectral analysis measures sedation and memory effects of propofol, midazolam, isoflurane, and alfentanil in healthy volunteers." *Anesthesiology*, **86**:836–847.

A. L. Goldberger, J. E. Mietus, D. R. Rigney, M. L. Wood, and S. M. Fortney (1994). "Effects of head-down bed rest on complex heart rate variability: response to LBNP testing." *Journal of Applied Physiology*, **77**(6):2863–2869.

P. Grassberger and I. Procaccia (1983). "Measuring the strangeness of strange attractors." *Physica D*, **9**:189–208.

H. Gray (2000). *Anatomy of the human body*. Bartleby.com, New York, online edition of the 20th edition. URL http://www.bartleby.com/107/.

R. Hamila, J. Astola, F. Alaya Cheikh, M. Gabbouj, and M. Renfors (1999). "Teager energy and the ambiguity function." *IEEE Transactions on Signal Processing*, **47**(1):260–262.

P. Hans, P.-Y. Dewandre, J. F. Brichant, and V. Bonhomme (2005). "Comparative effects of ketamine on Bispectral Index and spectral entropy of the electroencephalogram under sevoflurane anaesthesia." *British Journal of Anaesthesia*, **94**:336–340.

D. Harper (2001). "Online etymology dictionary." Web. URL http://www.etymonline.com/index.php. Last visited on 12.01.2007.

T. Higuchi (1988). "Approach to an irregular time series on the basis of the fractal theory." *Physica D*, **31**:277–283.

S.-L. Himanen, J. Virkkala, H. Huhtala, and J. Hasan (2002). "Spindle frequencies in sleep EEG show U-shape within first four NREM sleep episodes." *Journal of Sleep Research*, **11**:35–42.

S.-L. Himanen, J. Virkkala, E. Huupponen, and J. Hasan (2003). "Spindle frequency remains slow in sleep apnea patients throughout the night." *Sleep Medicine*, **4**:229–234.

K. Hirota, T. Kubota, H. Ishihara, and A. Matsuki (1999). "The effects of nitrous oxide and

ketamine on the Bispectral Index and 95% spectral edge frequency during propofol-fentanyl anaesthesia." *European Journal of Anaesthesiology*, **16**(11):779–783.

K. K. Ho, G. B. Moody, C. K. Peng, J. E. Mietus, M. G. Larson, D. Levy, and A. L. Goldberger (1997). "Predicting survival in heart failure case and control subjects by use of fully automated methods for deriving nonlinear and conventional indices of heart rate dynamics." *Circulation*, **96**(3):842–848.

W. E. Hoffman and G. Edelman (1995). "Comparison of isoflurane and desflurane anesthetic depth using burst suppression of the electroencephalogram in neurosurgical patients." *Anesthesia and Analgesia*, **81**(4):811–816.

R. Hornero, D. Abásolo, N. Jimeno, C. I. Sánchez, J. Poza, and M. Aboy (2006). "Variability, regularity, and complexity of time series generated by schizophrenic patients and control subjects." *IEEE Transactions on Biomedical Engineering*, **53**(2):210–218.

A.-M. Huotari, M. Koskinen, K. Suominen, S. Alahuhta, R. Remes, K. M. Hartikainen, and V. Jäntti (2004). "Evoked EEG patterns during burst suppression with propofol." *British Journal of Anesthesiology*, **92**(1):18–24.

T. Inouye, K. Shinosaki, H. Sakamoto, S. Toi, S. Ukai, A. Iyama, Y. Katsuda, and M. Hirano (1991). "Quantification of EEG irregularity by use of the entropy of the power spectrum." *Electroencephalography and Clinical Neurophysiology*, **79**:204–210.

L. C. Jameson and T. B. Sloan (2006). "Using EEG to monitor anesthesia drug effects during surgery." *Journal of Clinical Monitoring and Computing*, **20**(6):445–472.

H. H. Jasper (1958). "The ten-twenty electrode system of the International Federation." *Electroencephalography and Clinical Neurophysiology*, **10**:370–375.

E. W. Jensen, H. Litvan, M. Struys, and P. Martinez-Vazquez (2004). "Pitfalls and challenges when assessing the depth of hypnosis during general anesthesia by clinical signs and electronic indices." *Acta Anaesthesiologica Scandinavica*, **48**:1260–1267.

W. Jernajczyk, A. Sobańska, M. Marczak, A. Maciejewski, M. Latka, B. West, and M. Pokorski (2006). "The influence of acute progressive hypoxia on bioelectrical activity of the brain." *Journal of Physiology and Pharmacology*, **57 Suppl 4**:165–174.

V. Jäntti, A. Yli-Hankala, G. A. Baer, and T. Porkkala (1993). "Slow potentials of EEG burst suppression pattern during anaesthesia." *Acta Anaesthesiologica Scandinavica*, **37**(1):121–123.

D. J. Jones and T. W. Parks (1992). "A resolution comparison of several time-frequency representations." *IEEE Transactions on Signal Processing*, **40**:413–420.

D. L. Jones and R. G. Baraniuk (1995). "An adaptive optimal-kernel time-frequency representstion." *IEEE Transactions on Signal Processing*, **43**:2361–2371.

D. L. Jones and T. W. Parks (1990). "A high resolution data-adaptive time-frequency representation." *IEEE Transactions on Acoustics, Speech, and Signal Processing*, **38**:2127–2135.

D. Jordan, G. Schneider, A. Hock, T. Hensel, G. Stockmanns, and E. F. Kochs (2006). "EEG parameters and their combination as indicators of depth of anaesthesia." *Biomedizinische Technik. Biomedical engineering*, **51**:89–94.

H. Kantz and T. Schreiber (1997). *Nonlinear time series analysis.* Cambridge University Press.

W. Klonowski, E. Olejarczyk, and R. Stepien (2000). "Nonlinear dynamics of EEG-signal reveals influence of magnetic field on the brain." In "Proceedings of the 22th Annual EMBS

International Conference," pages 2955–2958. Chicago, IL.

M. Koskinen, T. Seppänen, S. Tong, S. Mustola, and N. V. Thakor (2006). "Monotonicity of approximate entropy during transition from awareness to unresponsiveness due to propofol anesthetic induction." *IEEE Transactions on Biomedical Engineering*, **53**(4):699–675.

J. P. Kress, A. S. Pohlman, M. F. O'Connor, and J. B. Hall (2000). "Daily interruption of sedative infusions in critically ill patients undergoing mechanical ventilation." *New England Journal of Medicine*, **342**(20):1471–1477.

K. J. Laidler (1995). *The physical world of chemistry.* Oxford University Press.

A. Lempel and J. Ziv (1976). "On the complexity of finite sequences." *IEEE Transactions on Information Theory*, **IT–22**:75–81.

T. Lipping, R. Ferenets, A. Anier, S. Melto, and S. Hovilehto (2005). "Power spectrum estimation in the calculation of spectral entropy to assess depth of sedation." In "The 3rd European Medical & Biological Engineering Conference," Prague, Czech Republic.

T. Lipping and V. Jäntti (2004). "EEG signal in monitoring brain function in anesthesia and intensive care: a review." *Proceedings of the Estonian Academy of Sciences: Engineering*, 10(2):95–109.

T. Lipping, V. Jäntti, and A. Yli-Hankala (2006). "Monitoring in anesthesia." In "Encyclopedia of Medical Devices and Instrumentation," , edited by J. G. Webster, volume 4, pages 555–565. John Wiley & Sons, Inc., Hoboken, New Jersey, 2nd edition.

E. N. Lorenz (1963). "Deterministic nonperiodic flow." *Journal of the Atmospheric Sciences*, 20:130–141.

P. J. Loughlin and L. Cohen (2004). "The uncertainty principle: global, local, or both?" *IEEE Transactions on Signal Processing*, **52**:1218–1227.

H. Lukatch and S. Greenwald (2003). *Neural mechanisms of anesthesia.*, chapter Cerebral cortex—anesthetic action on the electroencephalogram., pages 93–112. Humana Press, Inc., Totowa, New Jersey.

J. Machta (1999). "Entropy, information, and computation." *American Journal of Physics*, **67**:1074–1077.

A. Maksimow, M. Särkelä, J. W. Långsjö, E. Salmi, K. K. Kaisti, A. Yli-Hankala, S. Hinkka-Yli-Salomäki, H. Scheinin, and S. K. Jääskeläinen (2006). "Increase in high frequency EEG activity explains the poor performance of EEG Spectral Entropy monitor during S-ketamine anesthesia." *Clinical neurophysiology*, **117**:1660–1668.

S. Mallat (1999). *A wavelet tour of signal processing.* Academic Press, 2nd edition.

S. Mallat and Z. Zhang (1993). "Matching pursuit with time-frequency dictionaries." *IEEE Transactions on Signal Processing*, **41**:3397–3415.

D. A. McCormick and T. Bal (1997). "Sleep and arousal: thalamocortical mechanisms." *Annual Review of Neuroscience*, 20:185–215.

R. D. Miller, editor (2000). *Anesthesia*, volume 2. Churchill Livingstone, 5th edition.

T. H. Mäkikallio, T. Seppänen, K. E. Airaksinen, J. Koistinen, M. P. Tulppo, C. K. Peng, A. L. Goldberger, and H. V. Huikuri (1997). "Dynamic analysis of heart rate may predict subsequent ventricular tachycardia after myocardial infarction." *American Journal of Cardiology*,

80(6):779–783.

M. F. Murphy (1996). "Sedation." *Annals of Emergency Medicine*, **27**(4):461–463.

G. Mychaskiw, M. Horowitz, V. Sachdev, and B. J. Heath (2001). "Explicit intraoperative recall at a Bispectral Index of 47." *Anesthesia and Analgesia*, **92**(4):808–809.

S. A. Nasraway, E. C. Wu, R. M. Kelleher, C. M. Yasuda, and A. M. Donnelly (2002). "How reliable is the Bispectral Index in critically ill patients? A prospective, comparative, single-blinded observer study." *Critical Care Medicine*, **30**(7):1483–1487.

L. E. Nelson, T. Z. Guo, J. Lu, C. B. Saper, N. P. Franks, and M. Maze (2002). "The sedative component of anesthesia is mediated by $GABA_A$ receptors in an endogenous sleep pathway." *Nature Neuroscience*, **5**(10):979–984.

E. Niedermayer (1999). "The Normal EEG of the waking adult." In "Electroencephalography: Basic Principles, Clinical Applications, and Related Fields," , edited by E. Niedermayer and F. Lopes da Silva, pages 147–173. Williams & Wilkins, Baltimore, USA, 4th edition.

M. Parts, T. Lipping, J. Lass, and H. Hinrikus (2003). "Bispectrum for the detection of the effect of photic and microwave stimulation on human EEG." In "Proceedings of the 25th Annual International Conference of the IEEE," volume 3, pages 2327–2330.

D. T. Pham (1996). "Blind separation of instantaneous mixture of sources via an independent component analysis." *IEEE Transactions on Signal Processing*, **44**:2768–2779.

D. T. Pham (2004). "Fast algorithms for mutual information based independent component analysis." *IEEE Transactions on Signal Processing*, **52**:2690–2700.

S. M. Pincus (1991). "Approximate entropy as a measure of system complexity." *Proceedings of the National Academy of Sciences*, **88**:2297–2301.

S. M. Pincus, I. M. Gladstone, and R. A. Ehrenkranz (1991). "A regularity statistic for medical data analysis." *Journal of Clinical Monitoring*, **7**:335–345.

S. M. Pincus and A. L. Goldberger (1994). "Physiological time-series analysis: what does regularity quantify?" *American Journal of Physiology*, **266**(4 Pt 2):H1643–H1656.

G. E. Powell and I. C. Percival (1979). "A spectral entropy method for distinguishing regular and irregular motion of Hamiltonian systems." *Journal of Physics A*, **12**:2053–2071.

N. Radhakrishnan and B. N. Gangadhar (1998). "Estimating regularity in epileptic seizure time-series data. A complexity-measure approach." *IEEE engineering in medicine and biology magazine*, **17**:89–94.

S. E. Rampersad and M. F. Mulroy (2005). "A case of awareness despite an "adequate depth of anesthesia" as indicated by a Bispectral Index monitor." *Anesthesia and Analgesia*, **100**(5):1363–1364.

I. J. Rampil (1998). "A primer for EEG signal processing in anesthesia." *Anesthesiology*, **89**:980–1002.

M. Ramsay, T. Savege, and B. Simpson (1974). "Controlled sedation with alphaxolene/alphadalone." *British Medical Journal*, **2**:656–659.

R. Rautee, T. Sampson, M. Särkelä, S. Melto, S. Hovilehto, and M. van Gils (2004). "Application of spectral entropy to EEG and facial EMG frequency bands for the assessment of level of sedation in ICU." In "Proceedings of the 26th IEEE EMBS Annual International

Conference," pages 3481–3484. San Francisco, USA.

A. Recart, I. Gasanova, P. F. White, T. Thomas, B. Ogunnaike, M. Hamza, and A. Wang (2003). "The Effect of Cerebral Monitoring on Recovery After General Anesthesia: A Comparison of the Auditory Evoked Potential and Bispectral Index Devices with Standard Clinical Practice." *Anesthesia and Analgesia*, **97**(6):1667–1674.

A. Rényi (1995). "On a new axiomatic theory of probability." *Acta Math. Hungar.*, **6**:285–335.

I. A. Rezek and S. J. Roberts (1998). "Stochastic complexity measures for physiological signal analysis." *IEEE Transactions on Biomedical Engineering*, **45**(9):1186–1191.

J. S. Richman and J. R. Moorman (2000). "Physiological time-series analysis using approximate entropy and sample entropy." *American journal of physiology. Heart and circulatory physiology*, **278**:2039–2049.

M. L. Riess, U. A. Graefe, C. Goeters, H. V. Aken, and H. G. Bone (2002). "Sedation assessment in critically ill patients with Bispectral Index." *European Journal of Anaesthesiology*, **19**(1):18–22.

A. Roth-Isigkeit, J. Brechmann, L. Dibbelt, H. H. Sievers, W. Raasch, and P. Schmucker (1998). "Persistent endocrine stress response in patients undergoing cardiac surgery." *Journal of Endocrinological Investigation*, **21**(1):12–19.

U. Rudolph and B. Antkowiak (2004). "Molecular and neuronal substrates for general anaesthetics." *Nature Reviews Neuroscience*, **5**(9):709–720.

B. Schultz, A. Schultz, and U. Grouven (2000). "Sleeping stage based systems (Narcotrend)." In "New Aspects of High Technology in Medicine," , edited by H. Bruck, F. Koeckerling, F. Bouchard, and C. Schug-Paß, pages 285–291. Monduzzi Editore, Bolognia.

L. Senhadji, E. Wodey, and E. Claude (2002). "Monitoring approaches in general anesthesia: a survey." *Critical Reviews In Biomedical Engineering*, **30**:85–97.

C. E. Shannon (1948). "A mathematical theory of communication." *The Bell System Technical Journal*, **27**:379–423, 623–656.

B. A. Shapiro (1999). "Bispectral Index: better information for sedation in the intensive care unit?" *Critical Care Medicine*, **27**(8):1663–1664.

F. Sharbrough, G.-E. Chatrian, R. P. Lesser, H. Liiders, M. Nuwer, and T. W. Pictor (1991). "American Electroencephalographic Society guidelines for standard electrode position nomenclature." *Journal of Clinical Neurophysiology*, **8**:200–202.

H.-C. Shin, S. Tong, S. Yamashita, X. Jia, R. G. Geocadin, and N. V. Thakor (2006). "Quantitative EEG and effect of hypothermia on brain recovery after cardiac arrest." *IEEE Transactions on Biomedical Engineering*, **53**(6):1016–1023.

J. W. Sleigh and J. P. M. Barnard (2004). "Entropy is blind to nitrous oxide. Can we see why?" *British Journal of Anaesthesia*, **92**:159–161. (Editorial).

J. W. Sleigh, D. A. Steyn-Ross, M. L. Steyn-Ross, C. Grant, and G. Ludbrook (2004). "Cortical entropy changes with general anaesthesia: theory and experiment." *Physiological Measurement*, **25**:921–934.

N. J. Smith, M. van Gils, and P. Prior, editors (2006). *Neurophysiological monitoring during intensive care and surgery.* Elsevier.

H. M. Soliman, C. Mélot, and J. L. Vincent (2001). "Sedative and analgesic practice in the intensive care unit: the results of a European survey." *British Journal of Anaesthesia*, **87**(2):186–192.

M. Steriade, F. Amzica, and D. Contreras (1994). "Cortical and thalamic cellular correlates of electroencephalographic burst-suppression." *Electroencephalography and Clinical Neurophysiology*, **90**(1):1–16.

M. Steriade and I. Timofeev (2003). "Neuronal plasticity in thalamocortical networks during sleep and waking oscillations." *Neuron*, **37**(4):563–576.

D. F. Styer (2000). "Insight into entropy." *American Journal of Physics*, **68**:1090–1096.

B. E. Swartz and E. S. Goldensohn (1998). "Timeline of the history of EEG and associated fields." *Electroencephalography and Clinical Neurophysiology*, **106**(2):173–176.

J. Szczepański, J. M. Amigó, E. Wajnryb, and M. V. Sanches-Vives (2003). "Application of Lempel-Ziv complexity to the analysis of neural discharges." *Network: Computation in Neural Systems*, **14**:335–350.

N. V. Thakor, H.-C. Shin, S. Tong, and R. G. Geocadin (2006). "Quantitative EEG assessment." *IEEE Engineering In Medicine and Biology Magazine*, **25**(4):20–25.

P. H. Tonner, A. Paris, and J. Scholz (2006). "Monitoring consciousness in intensive care medicine." *Best Practice & Research Clinical Anaesthesiology*, **20**(1):191–200.

P. H. Tonner, N. Weiler, A. Paris, and J. Scholz (2003). "Sedation and analgesia in the intensive care unit." *Current Opinion in Anaesthesiology*, **16**(2):113–121.

G. Tononi and G. M. Edelman (1998). "Consciousness and complexity." *Science*, **282**:1846–1851.

M. Tribus and E. C. McIrvine (1971). "Energy and information." *Scientific American*, **225(3)**:179–188.

C. Tsallis (2002). "Entropic nonextensivity: a possible measure of complexity." *Chaos, Solitons, & Fractals*, **13**:371–391.

A. Vakkuri, A. Yli-Hankala, R. Sandin, S. Mustola, S. Høymork, S. Nyblom, P. Talja, T. Sampson, M. van Gils, and H. Viertiö-Oja (2005). "Spectral entropy monitoring is associated with reduced propofol use and faster emergence in propofol-nitrous oxide-alfentanil anesthesia." *Anesthesiology*, **103**:247–249.

A. Vakkuri, A. Yli-Hankala, P. Talja, S. Mustola, H. Tolvanen-Laakso, T. Sampson, and H. Viertiö-Oja (2004). "Time-frequency balanced spectral entropy as a measure of anesthetic drug effect in central nervous system during sevoflurane, propofol, and thiopental anesthesia." *Acta Anaesthesiologica Scandinavica*, **48**:145–143.

M. van de Velde (2000). *Signal validation in electroencephalography research.* Ph.D. thesis, Eindhoven University of Technology, Eindhoven, the Netherlands.

M. van Gils, I. Korhonen, and A. Yli-Hankala (2002). "Methods for assessing adequacy of anesthesia." *Critical Reviews In Biomedical Engineering*, **30**:103–118.

C. H. Vanderwolf (2000). "Are neocortical gamma waves related to consciousness?" *Brain Research*, **855**(2):217–224.

H. E. M. Vereecke, M. M. R. F. Struys, and E. P. Mortier (2003). "A comparison of Bispectral Index and ARX-derived auditory evoked potential index in measuring the clinical interaction

between ketamine and propofol anaesthesia." *Anaesthesia*, **58**(10):957–961.

H. Viertiö-Oja, V. Maja, M. Särkelä, P. Talja, N. Tenkanen, H. Tolvanen-Laakso, M. Paloheimo, A. Vakkuri, A. Yli-Hankala, and P. Meriläinen (2004). "Description of the Entropy™ Algorithm as applied in the Datex-Ohmeda S/5™ Entropy Module." *Acta Anaesthesiologica Scandinavica*, **48**:154–161.

J. Ville (1948). "Théorie et applications de la notion de signal analytique." *Câbles et Transm.*, **2A**(1):61–74.

A. D. Watts, I. A. Herrick, R. S. McLachlan, R. A. Craen, and A. W. Gelb (1999). "The effect of sevoflurane and isoflurane anesthesia on interictal spike activity among patients with refractory epilepsy." *Anesthesia and Analgesia*, **89**(5):1275–1281.

E. P. Wigner (1932). "On the quantum correction for thermodynamic equilibrium." *Physical Review*, **40**:749–759.

W. J. Williams (1996). "Reduced interface distributions: biological applications and interpretations." *Proceedings of the IEEE*, **84**(6):1264–1280.

S. Wolter, C. Friedel, K. Böhler, U. Hartmann, W. J. Kox, and M. Hensel (2006). "Presence of 14Hz spindle oscillations in the human EEG during deep anesthesia." *Clinical Neurophysiology*, **117**(1):157–168.

X.-G. Xia, Y. Owechko, B. H. Soffer, and R. M. Matic (1996). "On generalized-marginal time-frequency distributions." *IEEE Transactions on Signal Processing*, **44**:2882–2886.

J. Xu, Z. R. Liu, R. Liu, and Q. F. Yang (1997). "Information transformation in human cerebral cortex." *Physica D*, **106**:363–74.

X. S. Zhang and R. J. Roy (1999). "Predicting movement during anaesthesia by complexity analysis of electroencephalograms." *Medical and Biological Engineering And Computing*, **37**(3):327–334.

X.-S. Zhang and R. J. Roy (2001). "Derived fuzzy knowledge model for estimating the depth of anesthesia." *IEEE Transactions of Biomedical Engineering*, **48**:312–323.

X.-S. Zhang, R. J. Roy, and E. W. Jensen (2001). "Eeg complexity as a measure of depth of anesthesia for patients." *IEEE Transactions of Biomedical Engineering*, **48**:1424–1433.

J. Żygierewicz (2000). *Analysis of sleep spindles and model of their generation.* Ph.D. thesis, Warsaw University, Warsaw, Poland.

Tampereen teknillinen yliopisto
PL 527
33101 Tampere

Tampere University of Technology
P.O. Box 527
FIN-33101 Tampere, Finland